ESTIMATE CHARACTERISTICS OF OPEN GRADED FRICTION COURSES BY DIGITAL IMAGE ANALYSIS

Kasun Vimukthi Dedigamuwa

198109N

Degree of Master of Science

Department of Civil Engineering

University of Moratuwa

Sri Lanka

December 2021

ESTIMATE CHARACTERISTICS OF OPEN GRADED FRICTION COURSES BY DIGITAL IMAGE ANALYSIS

Kasun Vimukthi Dedigamuwa

198109N

Thesis submitted in partial fulfilment of the requirements for the degree Master of Science in Civil Engineering

Department of Civil Engineering

University of Moratuwa

Sri Lanka

December 2021

DECLARATION

I declare that this is my own work and this thesis does not incorporate without acknowledgement any material previously submitted for a Degree or Diploma in any other university or institute of higher learning and to the best of my knowledge and belief, it does not contain any material previously published or written by another person except where the acknowledgement is made in the text.

In addition, I hereby grant University of Moratuwa the non-exclusive right to reproduce and distribute the thesis, in whole or in part in print, electronic or other medium. I retain the right to use this content in whole or part in future works (such as articles or books).

Signature: Date: 17/12/2021

The above candidate has carried out research for the Master of Science under my supervision

Name of the supervisor: Prof. W. K. Mampearachchi

Signature of the supervisor: Date: 17/12/2021

ACKNOWLEDGEMENT

During the period of my postgraduate research degree, I had the opportunity to gain knowledge, skills and experience to apply the experimental and analytical phases of the research to produce significantly important findings for the well-being of the community.

There are few numbers of persons, I must pay my gratitude for their help and support on successful completion of my research.

First, I am very obliged of the guidance, knowledge and the experience given and shared by my research supervisor Prof. W. K. Mampearachchi, Professor of Civil Engineering, Department of Civil Engineering University of Moratuwa. Then I would like to thank my research chairperson and the research coordinator, Dr. H. R. Pasindu, Senior lecturer, Department of Civil Engineering University of Moratuwa and Prof. R. U. Halwathura, Professor, Department of Civil Engineering, University of Morauwa for evaluating and guiding me towards valuable outcomes during the progress review presentations and meetings. Further, I would like to extend my gratitude several personnel of non- academic staff of Department of Civil Engineering of University of Moratuwa; Mr. Leenas, Mr. Udith and Mr. Pathum for supporting my laboratory experiments.

Finally, I would like to thank my wife, Anuradha for supporting me on academic work as well as non-academic works to make my life much easier. Finally, I would thank my parents for all the support they have given me from the beginning to where I am now.

K. V. Dedigamuwa,

Department of Civil Engineering,

University of Moratuwa.

17/12/2021

ABSTRACT

The application of Open Graded Friction Courses (OGFC) as a pavement material has become a suitable solution for areas with high rainfall intensities. Since, OGFC material can act as a function-oriented pavement material to enhance permeability, reduce noise, and introduce more friction, improving the properties OGFC asphalt material to meet the requirements has drawn the attention of researchers in the last few decades. It is evident that the existence of a complex interconnected void network in OGFC has directly affected the durability and the permeability of the mixture. Further, the interconnected void network entirely depends upon the internal aggregate arrangement. Therefore, the identification of the internal arrangement of aggregates is very important to understand the void structure and improve the performance of designing OGFC. The lack of availability of quality controlling tools in the industrial construction stage leads to the occurrence of defects at the service stage and most of these issues can be minimized by investigating the internal structure of OGFC. This study presents a cost effective, rapid Digital Image Processing (DIP) method to determine the internal aggregate structure and the gradations of a core sample during the design and construction stages. Further, the proposed method enables the identification and quantification of segregation variation, internal voids and material distribution along the depth of the specimen. Experimental program of the study majorly included permeability test and durability test to compare the analytical results obtained for validation and justification. The internal aggregate structure data was collected by capturing cross section images in order to introduce a feasible way of implementing a gradation analysis. The cross sectional details were analysed to obtain details of areas, lengths and coordinates by developing an algorithm in MATLAB software. MATLAB was also used to obtain 2D aggregates structures and 3D models of specimens were constructed by using the python tool “plotly” on “Anaconda” platform. This research provides fundamentals to interpret and analyse data using DIP to construct the internal aggregate structure of OGFC specimens to identify and quantify deviations by the means of gradation, segregation and voids.

Keywords: Digital Image Processing, Gradation, Internal Structure, MATLAB, OGFC

LIST OF PUBLICATIONS

Conference Publications

1. Title: Analysing the Durability and the Lateral Drainage Characteristics of Open Graded Friction Course Pavement

   Conference: International Conference on Civil Engineering and Applications 2019

Journal Publications

1. Road Materials and Pavement Design (Under Review)
   Title: Analysis of the Spatial Distribution of Aggregate Gradations of Open Graded Friction Courses by Digital Image Processing

CONTENT

TABLES

FIGURES

1. INTRODUCTION

1.1 Background

The increase of automobile needs has majorly influenced the development of pavement engineering. The development of automobile industry has accelerated with the increase of ownerships of vehicles and to meet the required heavy traffic conditions, the pavements technologies has been introduced and enhanced in all over the world(Liu et al., 2020). As a result, many single granular roads were transformed to multilane asphalt roads with standardized features within few decades(Coleman O'Flaherty, 2015). As the asphalt technology enhanced, aspects such as innovative materials(Pereira & Pais, 2017), new methods of construction, standardized design methods, different traffic needs, and environmental conditions were considered and researched separately and jointly. When the different aspects were considered, it was found that variation in the gradation provides pavement materials with different properties. Considering different gradations, there were mainly three different types of asphalt; dense-graded, gap-graded and open-graded(Fang et al., 2019). Dense graded asphalts has been commonly used in most occasions due to its higher stability compared to the other two types. The gap-graded asphalt commonly contains higher fine content that usually provides the highest durability and the lowest permeability.

However, providence of an altered internal structure and a surface compared to other two types makes open-graded asphalt different. Usually, the internal structure of open-graded asphalts consist with a higher percentage of void content that makes the layer highly permeable(Alvarez et al., 2010). The irregular texture of the surface of open-graded asphalts provides higher friction compared to other two types. Therefore, this material was generally named as open graded friction courses (OGFC).

Although the dense-graded has been commonly used, OGFC has shown many advantages under wet weather conditions due to the porous nature of the structure of asphalt by reducing risks related poor visibility(Pathak et al., 2020), less friction and hydroplaning(Zhu et al., 2017). Typically, OGFC provides benefits such as high friction, reduced splashing(King et al., 2013) under wet weather conditions, and reduced asphalt surface shine for better visibility, better horizontal drainage through irregular surface, and better vertical drainage through the highly permeable internal

structure, enhanced skid resistance(Alvarez-Lugo et al., 2014), noise reduction(Lan Wang et al., 2009) and reduced hydroplaning.

As OGFC provides many benefits under the given conditions, the major reasons to under use OGFC is the low durability of OGFC. Even though, the OGFC layer durability has a considerable lifetime, the lifetime of the benefits provided by OGFC usually fade in a lower period(Anderson et al., 2013). After that period, OGFC will only provide the benefits of a typical asphalt layer, which leads to arise the issues mitigated initially such as high noise levels and low permeability. Moreover, the total lifetime of OGFC has been typically less than that of a dense graded asphalt. Therefore, one of the outputs of this research is to initiate a method to understand how to enhance OGFC in above flaws.

This porous nature of OGFC depends on the ratio of the proportions of fine and coarser aggregates. Although, the interlocking of aggregates(Mampearachchi et al., 2019) of OGFC provides its structural strength to resist further deformation and disintegration, more durability can be obtained by altering fine and coarser aggregate ratio while considering the permeability requirements. The void content of OGFC plays a major role towards achieving an interconnected void structure, which has the capacity to drain water under considerable rain. The interconnected voids to total voids ratio has been observed while changing several parameters and carrying out mechanical testing procedures to creating a prediction model to design OGFC with less time and number of experiments [12]. However, it is difficult to analyse the internal structure of OGFC using traditional mechanical testing methods. Therefore, this study focused on a recent approach, Digital Image Processing (DIP) to analyse of the internal structure of OGFC with permeability and durability.

Although, DIP has been used for many decades on many engineering aspects, availability of the technology has vastly increased about two decades ago and during this period the enhancement of the technology and its accuracy has been elevated compared to the time before twentieth century. Several examples of DIP use in the field of highway materials can be shown as follows. Aggregate, void and mastic proportions of cast specimen were analysed and calculated to using X-ray images under DIP(Zelelew et al., 2008). Further, part of sieve analysis curves were reconstructed by use of images taken as a vertical section of several asphalt types using DIP with a certain

error(Reyes-Ortiz et al., 2021). Digital images of the top surfaced of specimens were used to evaluate the optimum bitumen content using perceptual image coding and neural network method (Mejias de Pernia & Gunaratne, 2017).

Therefore, this study is focused on capturing digital images of horizontal cross sections to carry out 2D analysis to construct 3D models of aggregate and voids networks by DIP using MATLAB and Python.

1.2 Research Significance

As a pavement material, OGFC still is needed to enhance stability and durability to increase for a reliable usage. Many of the different approaches made to enhance OGFC were traditional methods, which have not involved understanding the internal structure. Even though, the constitutions were known in quantities, the distribution and the arrangement of the constitutions in 3D space cannot be evaluated, grasped and predicted using these traditional mechanical methods. However, the distribution of the constitutions of a specimen can be analysed using digital image processing. Therefore, as a different approach, digital image processing was used in this research as an initiative to understand the internal structure of OGFC by the means of voids and aggregates distribution. This research provides different relationships among different parameters of OGFC and ways of illustrating the internal structure.

When comparing to the depths of the traditional methods has used to improve OGFC, digital image processing still are taking baby steps to enhance these areas. The main significance of this research is to initiate a method to understand the internal structures of OGFC specimens towards providing relationship to justify the experimental values of permeability and durability. However, the initiation, the customized programming specialized on direct obtaining of images and analysing data of OGFC is a preliminary stage and can lead to accomplish achieving enhanced OGFC in many aspects by improving the programs and hardware of image capturing.

1.3 Research Statement

Use of experimental and image processing techniques on evaluating durability and permeability of selected mixtures of open-graded friction courses to analyse relationships towards obtaining more durable and permeable as a pavement material.

1.4 Aim

To develop relationships among interconnected voids, total voids, permeability, durability characteristics of selected OGFC mixtures.

1.5 Objectives

The objectives were developed based on the aim defined for the study. The objectives are listed below.

- Creating 2D and 3D visual aids for better understanding the internal structure
- Gradation analysis to approximate the gradation of specimens
- Identification of horizontal segregation
- Identification of vertical segregation
- Relationships among voids, permeability and durability

1.6 Research Methodology

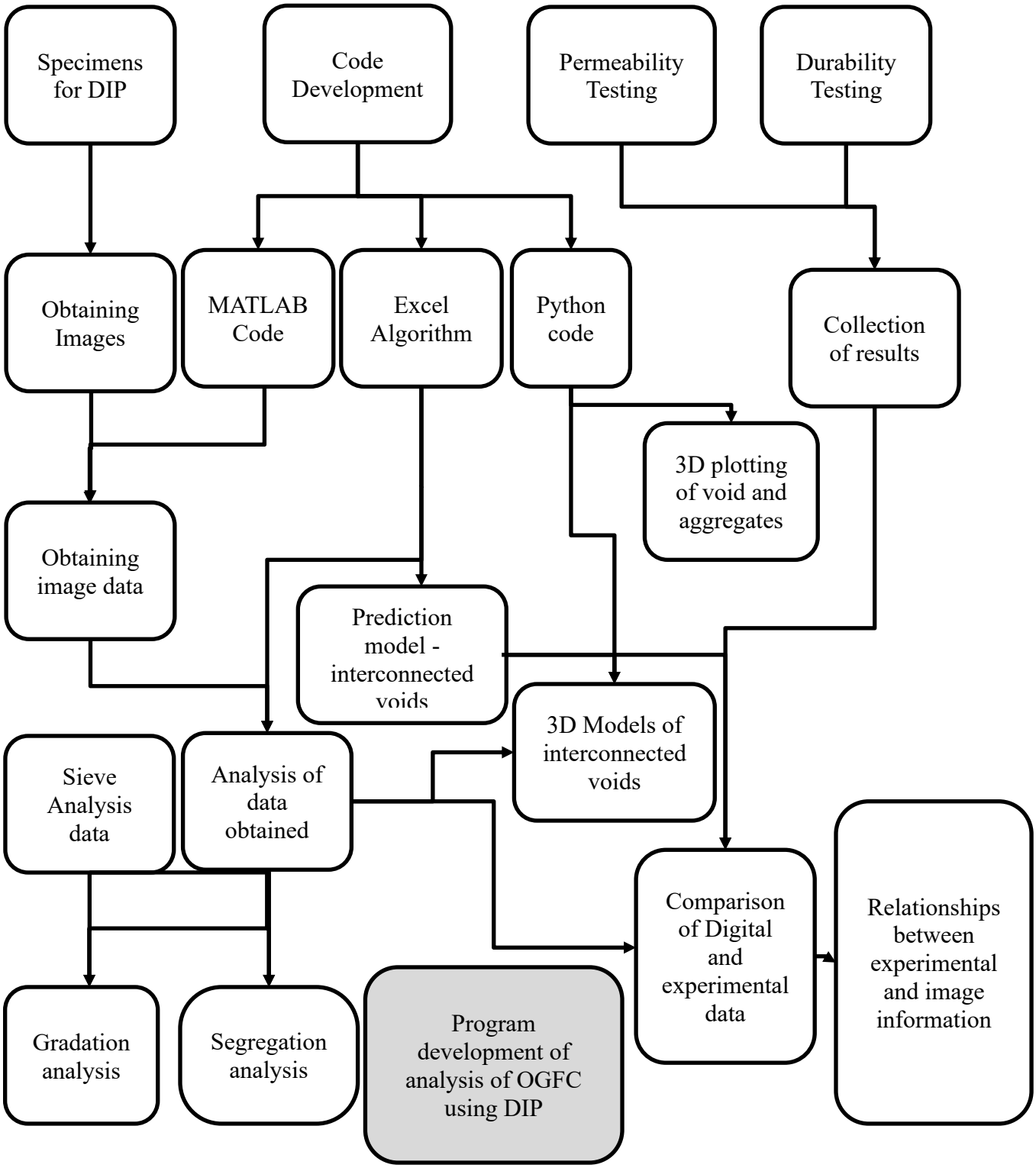

Figure 1.1: Research Methodology

The methodology in this study leads to developing a program to analyse OGFC core samples using DIP. This analysis would assist in analysing the horizontal and vertical segregation of aggregates, gradation prediction of a selected specimen, 3D voids structure arrangement, etc. How the major inputs and analyses such as image information, experimental data, MATLAB analysis, Python analysis, etc, leading and combining towards achieving major output of this research has been briefed explained in the Figure 1.1.

1.6.1 Experimental program

The experimental program was carried out based on the research gaps identified. The experiment program is listed below.

- Preparation of OGFC specimens
- Permeability test conducted according to the constant head method
- Durability test conducted accordance with Tex-241-F
- Development of photo booth apparatus to capture images
- Preparation of specimen for image capturing

1.6.2 Analytical model development program

This study required programming to knowledge in MATLAB and Python platforms. The program developed are listed below.

- Development of MATLAB codes
    - Identification of void and aggregate details
    - Development of Delaunay triangles
- Development of Excel algorithms
    - Algorithm development for predicted interconnected void models
    - Algorithm development for Delaunay distance calculations
    - Horizontal segregation analysis
- Development of Python codes
    - 3D models of aggregates and voids in specimen
    - 3D models of interconnected void networks

1.7 Outline of the Report

This report consists of four chapters. The chapter descriptions are as follows.

Chapter 1: Introduction

This chapter contains the background study, research significance, aims and objectives, and methodology of the research.

Chapter 2: Literature review

The literature available related to choosing and developing technologies and experiments have been widely discussed in this chapter

Chapter 3: Experimental program

The behaviour of durability and permeability of selected OGFC has been discussed. Further, to support image-processing analysis, image-obtaining techniques used have been discussed.

Chapter 4: Analytical model development program

This chapter explains how different programs were developed and used to obtain the required information to achieve objectives.

Chapter 5: Results and Discussion

The experimental test data results have been comprehensively discussed and analytical data extraction and processing have been explained. Further, comparison among experimental test results and analytical program has been discussed along with recommendations for potential future directions.

2. LITERATURE REVIEW

The status of knowledge investigation was highly supportive to set aims and objectives of this study. The literature review summarized here provided insights of the necessity of OGFC to the pavement industry, current implementation of OGFC, approaches on improving OGFC by DIP, etc.

2.1 Pros and cons of OGFC

OGFC is a pavement material, which provides a wide range of advantages, especially under wet weather condition. Along with the advancement of technology, it is a necessity to introduce specific types of asphalts such as OGFC in order to improve the quality of life. The following benefits of OGFC would lead to mitigate accidents and improve the average speed of vehicles. However, in order to achieve these benefits in the long run, the listed disadvantages below shall be addressed.

2.1.1 Horizontal drainage

Water does not remain on the surface of OGFC due to the porous nature of its structure. Surface of OGFC is usually made as a tire surface. Although the surface is flat, it has many irregularities that pass water through them without coming to the top of the surface of OGFC contacting the tire surface. Therefore, in rainy conditions, OGFC provides horizontal drainage through its irregularities without creating a water layer in between the tire and the road surface.

2.1.2 Vertical drainage

Vertical drainage of OGFC is also unique to OGFC. This allows water to move though the interconnected voids of the internal structure and disperse water through the edges of OGFC layers.

2.1.3 Condition after rain

Water will not remain on a surface of an OGFC even after a heavy rain due to its irregularity and porous nature. Therefore, soon after a rain, OGFC roads are safer than the other road types.

2.1.4 Reduction of hydroplaning, splashing and spraying

Typical dense graded or gap graded roads contains flats surfaces with low drainability leads to occur hydroplaning, splashing and spraying under rainy conditions. However, the contacting surface of OGFC to the tire is not much contained water as the irregularities fill the remaining water on the surface. Therefore, the tires will not contact with a higher water amount leads to have a low splashing and spraying. Hydroplaning on OGFC surfaces are highly unlikely due to not occurring of a water on OGFC surfaces under moderate rain conditions. However, with high intense rainy condition, even OGFC roads are not safe from hydroplaning effect.

2.1.5 Reduction of surface shine

Smooth road surfaces are tending to reflect the background to the driver by working as a mirror due to the smoothness of the surfaces. Examples can be given as smooth dense graded asphalt surfaces, gap graded asphalt surfaces and concrete surfaces. Further, a water film is usually created on these surfaces under rainy conditions. Therefore, under wet weather conditions, these roads tend to reflect more than it reflects under dry conditions (Figure 2.1).

OGFC roads do not provide deceiving reflections due to its irregularities on the surface. Even after the rains OGFC roads do not create a flat-water film. Therefore, the water remaining on OGFC surface will not support to create a water film, which is large enough to create deceiving reflections.

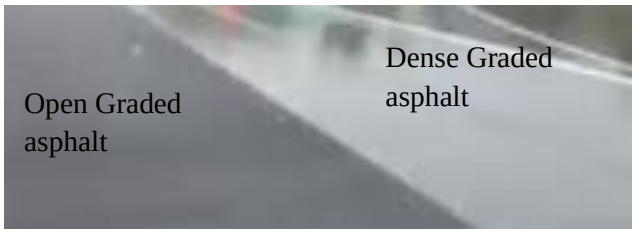

Figure 2.1:OGFC surface and dense graded surface under wet weather condition

2.1.6 Skid resistance

OGFC provides horizontal and vertical drainage in an enhanced way to avoid creating water film on its surface. Due to the higher micro textures and enhanced drainage, OGFC has low risks when it comes to hydroplaning(Zhu et al., 2017). Therefore, OGFC provides higher skid resistance compared to other many asphalt types.

2.1.7 High surface friction

Mirco-texture of OGFC surface usually depends on aggregate gradation and mixture design. OGFC surfaces makes coarser asphalt surfaces leading to achieve high micro textures than dense graded asphalt. Studies have shown that OGFC shows greater values of international friction index than typical dense graded asphalt (King et al., 2013).

2.1.8 Reduction of tire noises

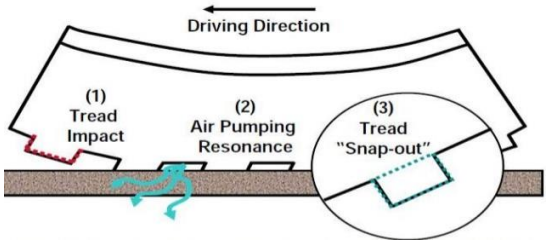

Figure 2.2: OGFC surface and dense graded surface under wet weather condition

The porous structure of OGFC creates an interconnected void network, which leads to every end of the pavement structure. The impact of the tire tread runs out through the pavement and the noise energy is absorbed to the pavement and the bottom layer if the pavement contents higher air voids as in OGFC. Therefore, the noise output from the OGFC pavement to the environment is lesser than the dense graded and gap graded asphalts. OGFC pavements have been used in some locations to reduce noises from the roads when the noise barrier was not allowed to construct.

A study conducted show that 40mm is the optimum OGFC layer thickness which can reduce maximal noise level when the flow of cars and trucks are considered (Lan Wang et al., 2009). Further, the study shows that OGFC layer can reduce maximal of 8.9dB noise level compared to dense graded asphalts.

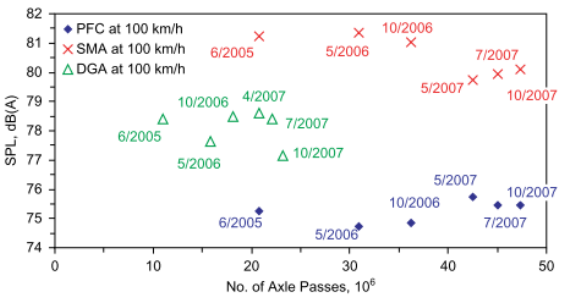

Figure 2.3: Noise level of different asphalt types (Kowalski et al., 2009)

2.1.9 Reduction of road temperature

Asphalt pavements usually tend to deteriorate with higher temperatures as the decay of bitumen accelerated. Many asphalt pavements are sheared with the vehicle breaking and movements under higher temperatures. Further, the pneumatic tires wear prematurely due to the use of high temperature roads. When the OGFC roads are used, the porous structure of the pavement retains water under the rainy conditions. This retained water is vaporized in high temperature conditions to maintain the temperature of the pavement low. This scenario will prevent pavement from accelerated deterioration and tires from vast consumption.

2.1.10 Clogging

Due to the porous structure of OGFC, the dust particles tent to move inside the pose and fill the void connections. Continuation of this process for a long period causes reduction of water movement inside the porous structure. This directly affects the permeability of OGFC.

A study shows that particle-related clogging of OGFC mixtures mainly caused by particles with critical sizes in the range of 0.15–0.3 and 1.18–2.36(J. Chen et al., 2015). These types of particles should be avoided on pavements to minimize the clogging of OGFC.

2.1.11 Rutting

OGFC contents void content around 15% to 25%. The structure of the pavement is structurally withstood by interlocking of coarser particles with each other. However, OGFC compacts further due to the axial forces given by the vehicles. Rutting of OGFC occurs faster than dense graded material. Further, the rutting depth are also high in OGFC compared to other asphalt types. A study conducted (Coleri et al., 2013) showed that before the heavy vehicle simulator (Load application) used, the void content of the specimen remained similar with the depth. However, after the heavy vehicle simulation, the void content gradually reduced from the bottom of the OGFC layer to the top of the OGFC layer with the depth. Permeability of the layer was reduced due to the reduction of voids in top of the OGFC layer. Many studies have shown that the rutting reduces the efficiently of many benefits of OGFC. Another study showed that with the

temperature of the pavement, the permeability changes under loading conditions. When the study conducted from temperatures from 15ºC to 35ºC, lowest permeability found at 35C indicates that with the increase of the temperature, the acceleration of rutting occurs(Hassan & Al-Jabri, 2005).

2.2 Usage of OGFC

USA experience

The cost benefit analysis conducted in Tennessee highways showed that it was cost-beneficial to use OGFC on their highway considering construction of pavement, driving safety and accident rates(X. Chen et al., 2017).

As according to a study conducted in Louisiana, Police reports showed a considerable reduction in accidents after laying of OGFC as shown in Table 2.1 (Kabir et al., 2012).

Table 2.1: Accident reduction according to Louisiana police

Route	Weather Condition	Number of Total Accidents/Year		Number of Fatalities/Year		Reduction in Total Accidents (%)	Reduction in Fatalities (%)
		Before	After	Before	After		
US-71	Wet	0.5	0.0	0.2	0.0	100	100
	All	2.0	0.2	0.2	0.0	92	100
I-20	Wet	28.6	6.8	0.6	0.0	76	100
	All	66.0	38.0	1.4	0.6	42	57
US-61	Wet	19.3	22.0	0.0	0.5	0	0
	All	175.6	191.5	1.1	1.5	0	0
US-171	Wet	1.6	0.7	0.0	0.0	57	0
	All	8.7	14.7	0.0	0.0	0	0

Another study conducted in USA showed that the lifetime of OGFC usually lies with five to ten years while having major drawback such as clogging, ravelling and winter maintenance problems(Onyango et al., 2017).

Japan experience

As shown in Figure 2.4, Japan roads have increased the use of OGFC in 20th century. This study shows that the accidents occur on same roads have been decreased by 85% after laying OGFC (Takahashi, 2013).

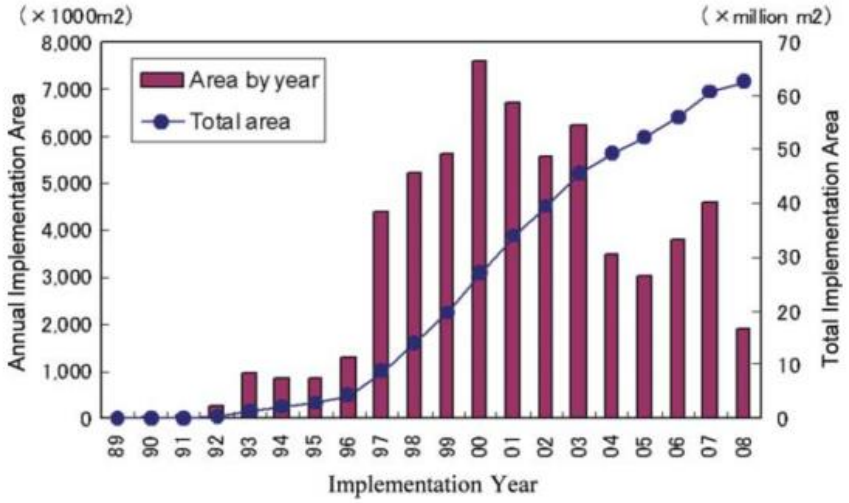

Figure 2.4: Usage of OGFC in Japan

2.3 Preparation of specimens

Although Marshal Method is quite commonly used in many countries for dense graded asphalts, Superpave method is being popular due to its multi-variable inclusive design approach and the compaction effort. Table 2.2 indicates the differences of the Superpave and Marshal compactors.

Table 2.2: Comparison between Marshal and Superpave compaction methods

Superpave Compactor`	**Marshal Compactor**
Impact and shear	Impact only
Can control compaction force	Cannot control compaction force
Can control compaction height	Cannot control compaction height
Only machinery	Manual and machinery
Modern method	Method practice in Sri Lanka

When it comes to the preparation of specimens using Superpave method, two standard diameters are used; 150 mm and 100 mm. In order to obtain a considerably larger area of a cross section of OGFC, 150 mm diameter Superpave standard size was selected.

2.4 Gradations of specimen

Different gradations of OGFC used in different projects and the performances of them in field were discussed (Figure 2.5).

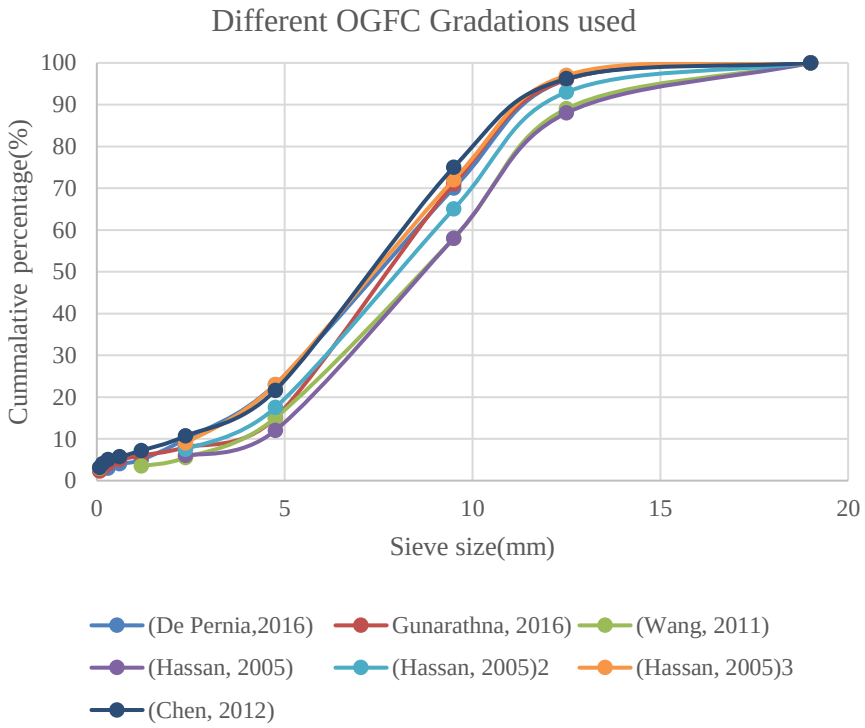

Figure 2.5: Different types of gradations used as OGFC (Y. Chen et al., 2012; Hassan & Al-Jabri, 2005; Mejias de Pernia & Gunaratne, 2017; Liang Wang et al., 2011)

2.5 Image data extraction and processing

There were many methods to analyse and model the behaviour of different constitutions of materials. All these methods supported to extract cross sectional data into digital numbers. Following can be given as examples for different methods and the tasks.

- Image Tool (developed by the Department of Dental Diagnostic Science at the University of Texas Health Science Centre) was used to characterize aggregates particles shape and orientation, and the Digital Image Analysis System (developed by the University of Wisconsin-Madison) was used to captures the

parameters that are related to HMA internal structural, which includes segregation, orientation and contact points respectively in the study (Bessa et al., 2012).

- To measure pavement surface failure, this study used MATLAB tools to extract image data and quantify the failure(Joni et al., 2020). This method can differentiate and quantify the pavement surface failure as percentages. Further, the program can be improved by increasing number of images used to train the program.
- A study carried out to related compaction and to the effect of aggregate interactions has been used MATLAB and C++ for data extraction and analysis purposes. This study has looked into many areas of object separation to equalizing, filtering and thresholding to enhance the image processing technique used(Kim & Kang, 2018).
- This study focused on reconstruction of sieve analysis curve of asphalt using a cross section. This particular cross section is obtained cutting the specimen vertically from top to bottom if its kept as cylinder as shown in the figure…..(Reyes-Ortiz et al., 2021). Aggregate areas obtained from the given cross sectional plane were accounted to reconstruct the sieve curve from the analysis. Program developed on MATLAB software was used to extract image data in this study.

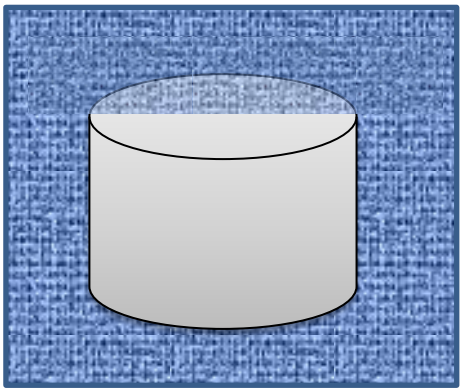

Figure 2.6: Cut section of the specimen used for this study

2.6 Illustration of 3D models

Even though many methods of data plotting are available, many platforms support 1D and 2D plotting. However, under Python programming on Jupytor notebook 3D (Kumar Rathore, 2017) data visualizations are possible as lines and objects. Basic guidance given under the website (3D Scatter Plots | Python | Plotly, 2021) was used on many applications such as to visualize how vaccines are powering the world's news cycles.

With the aid of Scatterplot_3D function in plotly, programs can be coded to visualize data in 3D space with different colours, shape and sizes. Another useful function called line_3d provides lines between give coordinates(3D Line Plots | Python | Plotly, 2021). The intensity and the colours of the lines can change according to the requirement.

3. EXPERIMENTAL PROGRAM

3.1 Overview

Three different OGFC gradations were selected and three samples from each gradation were prepared in cylindrical shapes having a diameter of 150 mm and a height of 60 mm. 50 standard gyrations were used on each specimen for compaction. Then, the samples were cut into slices. Then, the cross sectional surfaces were prepared to take images under a light-controlled environment.

3.2 Preparation of OGFC specimen

As shown in Table 3.1, three types of aggregate gradations and the corresponding bitumen contents were selected with minor differences to understand the relationships between permeability and durability. The bitumen type used to cast all the specimen types was PG 76-22. The Superpave Gyratory Compactor was used with 50 standard gyrations (Figure 3.2 (a)).

Figure 3.1: Specimens prepared to carry out durability test

150 mm and 60 mm height specimens were prepared for durability and permeability tests, respectively (Figure 3.1). 60 mm height specimens were used for image processing cross section analysis.

Table 3.1: Gradations of selected OGFC

	Sieve Size										
	19mm	12.5mm	9.5mm	4.75mm	2.36mm	1.18mm	600µm	300µm	150µm	75µm	OBC
A	100	95	74	20	8	6	4	4	4	3.4	5.50%
B	100	96	70	23	10	5	4	3	3	2.5	5.30%
C	100	96	71	15	8	6	5	4	3	2.3	5.30%

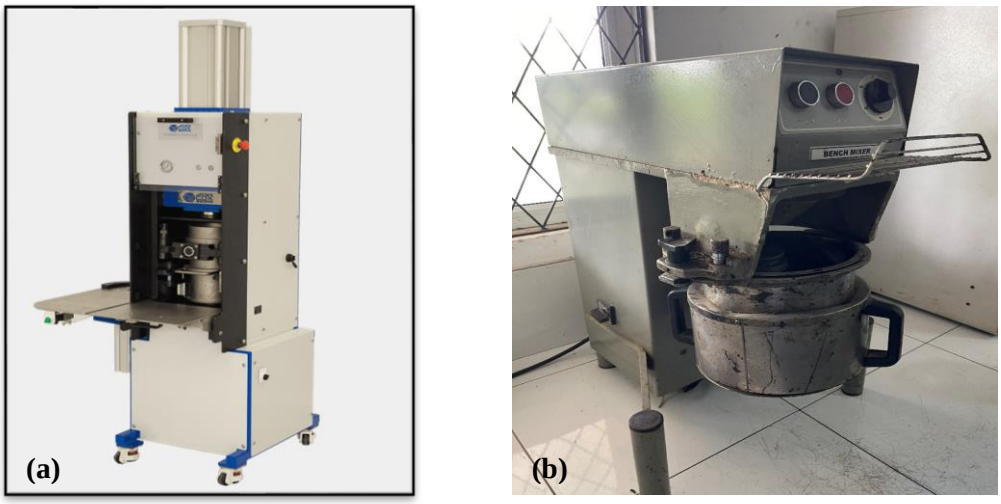

Figure 3.2: :(a) Superpave gyratory compactor (b) bench mixer

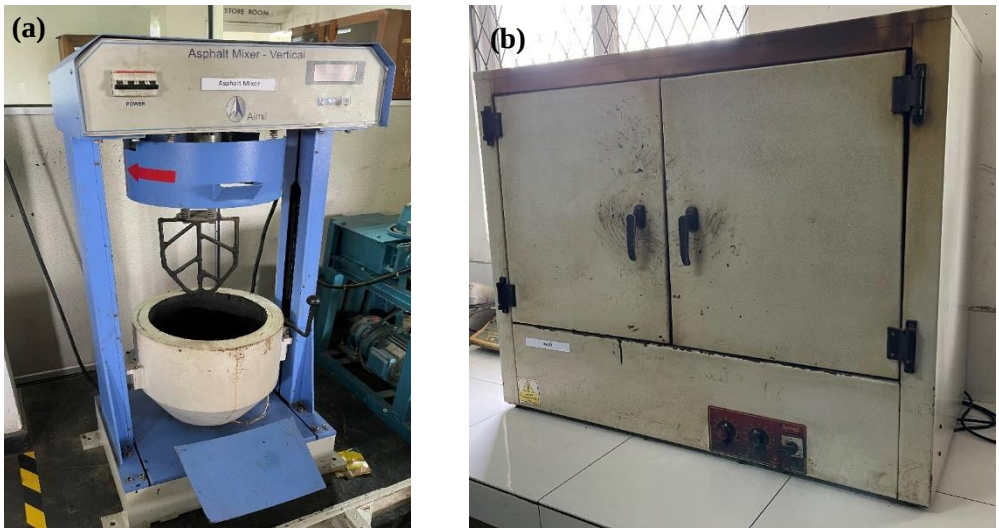

Figure 3.3: (a) Asphalt mixer (b) Oven

Modified bitumen and aggregate was heated in the oven at 175^0C (Figure 3.3(b)). The mixture weights less than 8kg were mixed in bench mixer (Figure 3.2(b)) and other

weights were mixed in asphalt mixer (Figure 3.3(a)). The temperature of the mixture was maintained at 160^0C and the mixturing was conducted for around 5 minutes to let aggregate surfaces to fully coated by bitumen. Heated mixture was then droped in to the heated mold.Mold is to be fixed to the Superpave gyratory compactor under safe mode switched on. The superpave gyratory compactor was operated using a computer based program. Therefore, the computer program was used to provide 50 gyrations to the mixture in the fixed mold. Followed by the application of gyrations, the hardened specimen was taken off from the mold after 18-24 hrs of air dried condition. Otherwise, the OGFC specimens would tend to deform from its original molded shape. Figure 3.1 shows the hardened formation of OGFC specimens.

3.3 Selection of void filler material

Selection of a proper void filler material was important to identify the interconnected voids separately. Therefore, a number of potential trail filler materials were used to fill OGFC specimens as shown in Figure 3.4. The observation collected from all filler materials are listed.

- Red cement– particle size was large. Therefore, could not seep through all visible interconnected voids. Initial setting was two and half-hours approximately.
- Waster base paint – The paint was not hardened inside the interconnected voids even after 3 days. This was due to the early hardening of top and bottom surface paints, hindering the water evaporation to harden the paint inside the interconnected voids.
- Resin – The resin and the bitumen started to melt and mix in such a way the aggregates became loosed. Due to the mixing of resin and the bitumen, the voids and bitumen seemed inseparable. Therefore, interconnected void areas could not be identified.
- Plaster of paris – Particle size was comparatively low. The setting time was less than 1 minute. Interconnected voids were clearly visible in white.

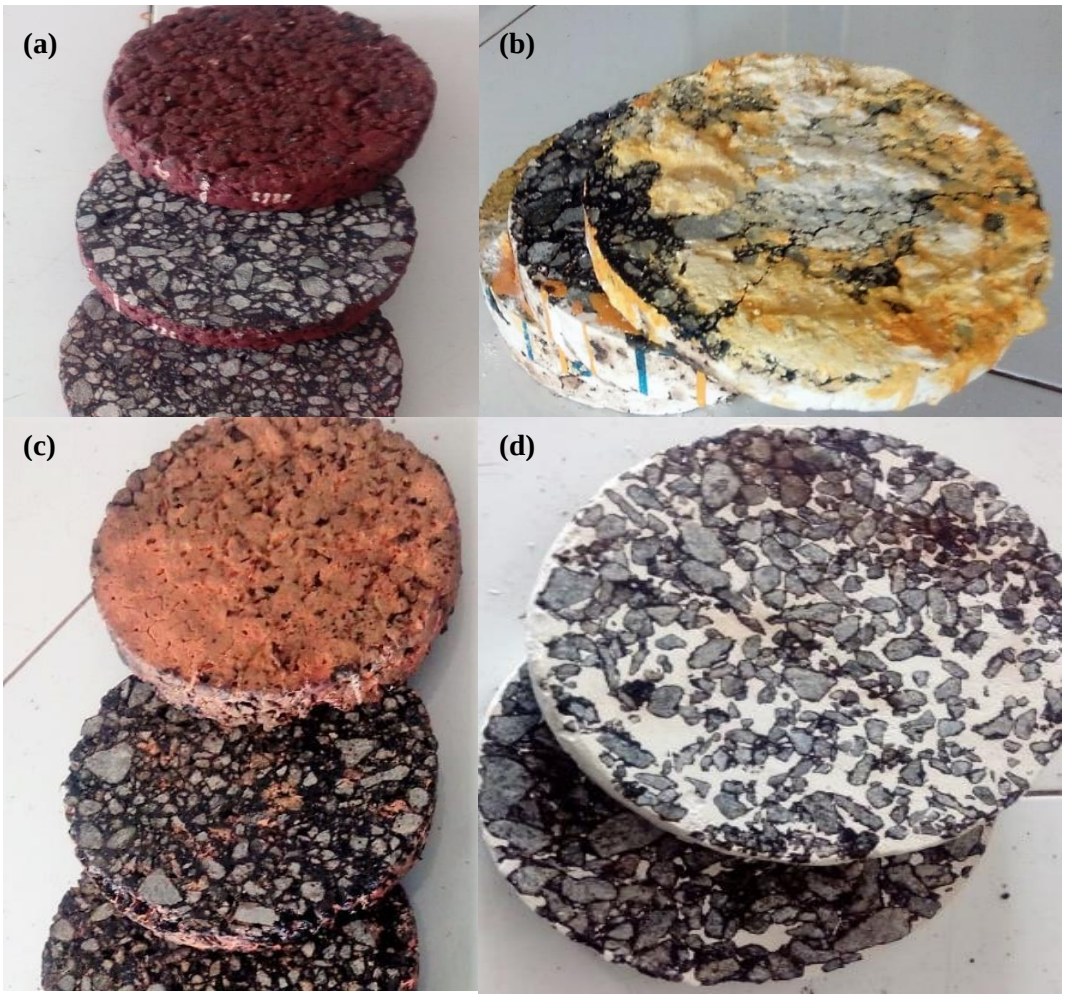

Figure 3.4: Trial filler materials used to fill interconnected voids (a) Red cement (b) Water based paint (c) Resin (d) Plaster of Paris

3.4 Permeability test

The permeability of a sample can be determined using the constant head method. In order to get an accurate average permeability value, different levels of constant heads can be maintained above the specimen. A permeability apparatus was developed according to ASTM C1754/1754M-12, to measure 150 mm diameter OGFC samples as shown in Figure 3.6. The apparatus was developed to collect flow rates at three different pressure heads.

- Details of the Permeability Apparatus

The sample retaining part was made of a steel tube having an inner diameter of 150 mm. The three pressure head maintaining outlets were situated 125 mm, 130 mm and 135 mm from the bottom of the sample retainer. Then the whole sample retainer is

partially submerged in a water bucket and the constant water head is maintained from the outlet from the bucket as shown in Figure 3.5.

- Sample preparation for the permeability test

  Before submerging the sample retainer in the water bucket, the OGFC sample has to be properly inserted into the sample retainer. First, Plaster of Paris has to be coated on the vertical curve wall of the OGFC sample. After the solidification of Plaster of Paris, the coated surface was smoothened to make an even surface. Then, the OGFC sample was inserted into a rubber tube to get an elastic flexible wall to fit into the sample retainer tightly. In order to ensure a proper seal between the wall of the sample retainer and the rubber wall, a silicon glue was applied. This seal was very important because, water seep through the pores in the OGFC sample was supposed to go out of the bucket outlet during the permeability test.

- The test

  The water seepage rate through the OGFC sample was measured by collecting a constant amount of water coming from the bucket outlet into a measuring cylinder and recording the time spent. The flow rates were recorded with respect to the water head provided. Nine flow rate recordings were collected altogether under three different water heads and average flow rate was taken as the permeability parameter for the specimen considered.

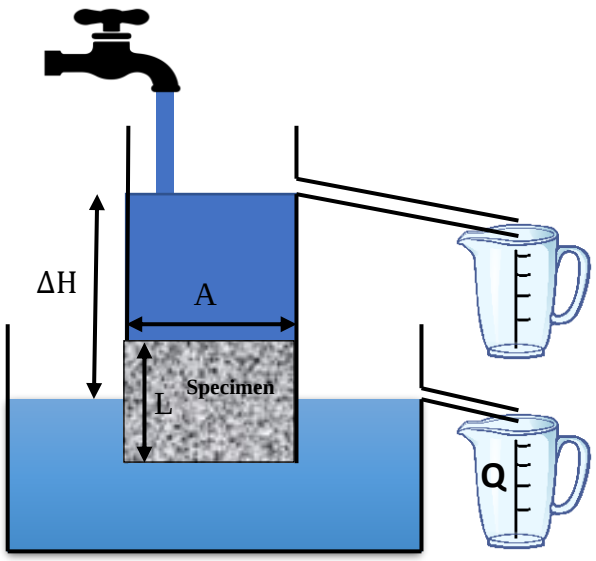

Figure 3.5: Permeability apparatus developed for this study

Figure 3.6: Specimen used for permeability test

3.5 Durability Test

The durability of OGFC can be measure by the Catabro test. The test apparatus is shown in Figure 3.7. This test method determines the abrasion loss of compacted asphalt specimens by the percentage of weight loss (Cantabro loss).

Figure 3.7: Los Angeles abrasion machine

Test procedure –

These specimens were prepared in accordance with TEX-241-F standard 150 mm diameter specimens. Before progressing with the Cantabro test, the samples were

weighed and that initial weights were recorded. Then a sample at a time was inserted to the apparatus after removing the steel balls in the apparatus. This steel ball removal from the apparatus is necessary for the Catabro test as instructed in the TEX-241-F standard. Then, the sample was subjected to 300 revolutions inside the Abrasion machine at a speed of 30-33 rpm. After the rotating process, the sample was taken out and brushed to remove discarded particles. Then the weight after the test was recorded and this procedure was carried out for three samples from each gradation.

3.6 Development of photo booth

This photo booth development was done to get the same light condition when capturing the cross sections of OGFC specimens. Image processing is majorly based on pixel area identification and therefore, it is necessary for any specific element in a considering cross-section shall be identical with another. As shown in Figure 3.8, the light controlling phot booth dimension was 2 feet x 2 feet in plan and 4 feet in height.

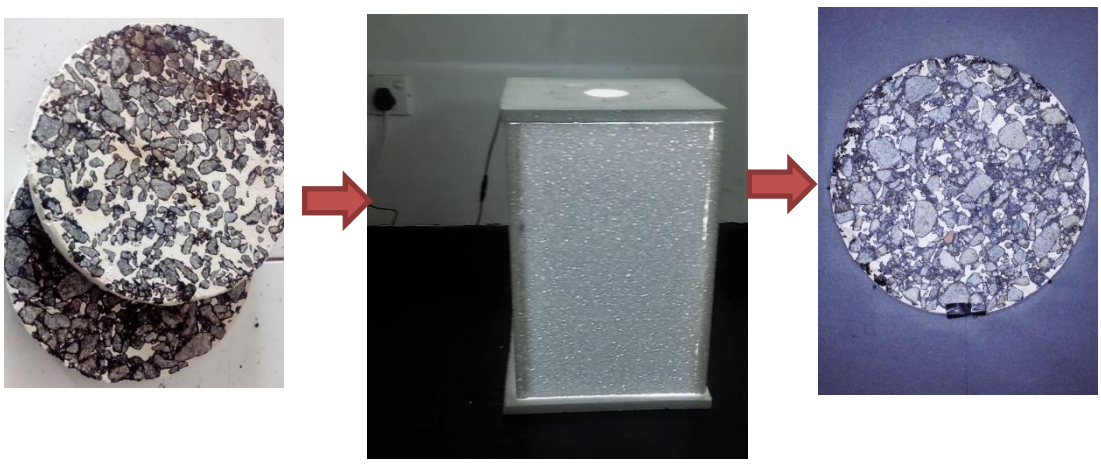

Figure 3.8: Cross sectional pieces to images by the developed photo booth

The photo booth was illuminated by a set of lights fixed on the upper part of the unit (Figure 3.9 (a)). The centre hole in Figure 3.9 (a) is there for the camera lens. The OGFC specimen was placed at the bottom of the photo booth. As indicated in Figure 3.9 (b), each specimen was kept on the exact location to minimize any light difference error.

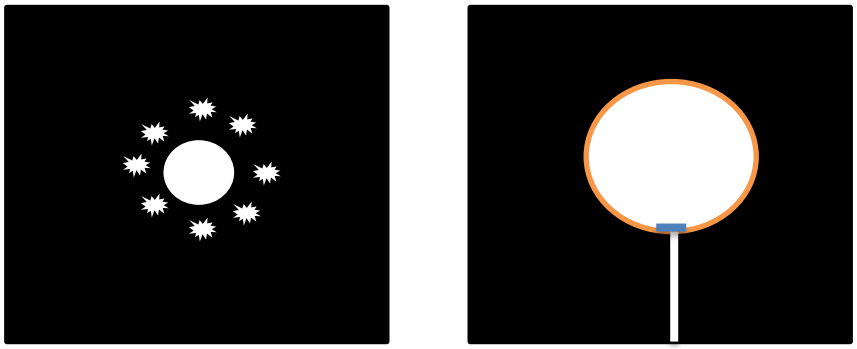

(a) **(b)**

Figure 3.9: (a) Top and (b) bottom inner sides of photo booth

3.7 Preparation of specimen for image capturing

In order to improve the visibility of interconnected voids of cross-sectional images at DIP stage, Plaster of Paris (PoP) was inserted to OGFC specimen. Prior to insertion of PoP, the irregular cylindrical surface (vertical) of the specimen was smoothened by coating PoP on it until there were no major irregularities on the cylindrical surface. Then, the PoP coated specimen was inserted into a rubber tube to make sure the flow of PoP did not seep out from the vertical wall of the specimen. Once the PoP was inserted to the top surface of the specimen, a vibratory action was provided to the specimen to speed up the insertion of PoP. Finally, the bottom of the sample was sealed and kept for 24 hours for the PoP to be solidified.

After the solidification of PoP, the excess material from top and bottom was removed and the circular surface was plastered with PoP to obtain a smooth surface. The sample orientation and the cutting locations were marked on the circular surface. Then, the sample was cut by a diamond cutter and the cut sections and surfaces was obtained as indicated in Figure 3.10 (a) and 3.10 (b) respectively.

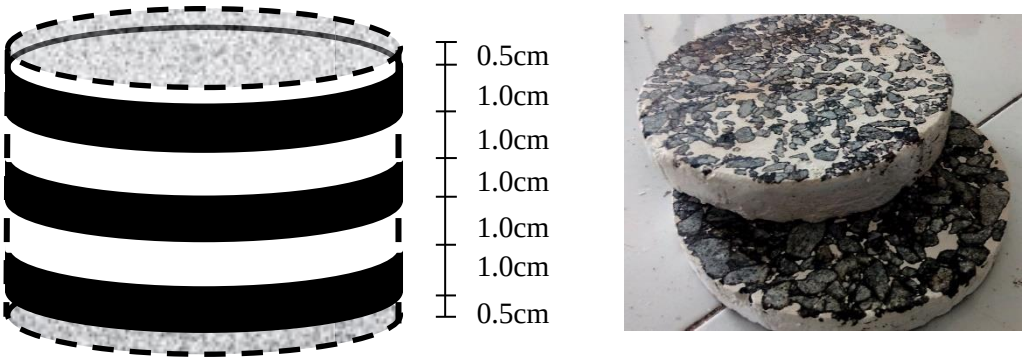

(a) (b)

Figure 3.10: The sample preparation for DIP (a) Cut sections of the specimen (b) Sliced sections

The top and the bottom surfaces of the cut slices of each specimen were captured using the DSLR camera under a controlled lighting environment. First, the orientation of the sample, the settings of the camera and the lighting intensity of the photo booth with lighting control were set up to obtain the images with same exposure and same colour conditions.

There are three major components in analytical model as shown in Figure 4.1. Image extraction is completely carried out using MATLAB and 3D models were completely developed on python. All the major analysis were carried out by using MATLAB and excel platforms. The analytical model is comprehensively discussed below.

4. ANALYTICAL MODEL

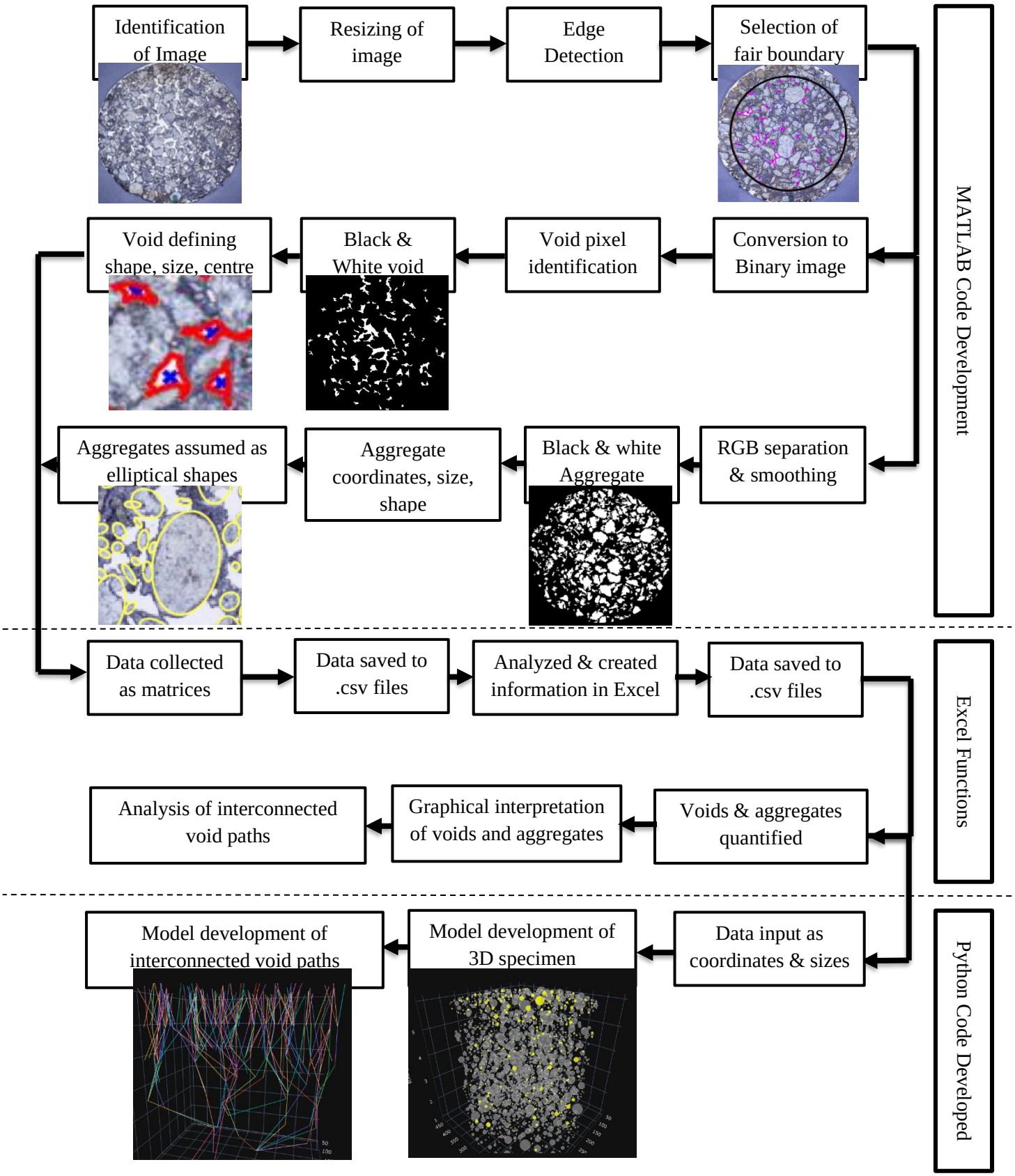

Figure 4.1: Analytical model development diagram

4.1 Image data extraction

In order to extract data, image capture from light booth were cropped and arranged to the required order using Lightroom software. After that, the enhanced images were copied to the folder, which is used to save the input data to the MATLAB program.

4.1.1 MATLAB program on extraction of image data

The code required for the data extraction is explained extensively under 4.1.1.1 section. Thereafter the inputs and the outputs of one execution is explained as an example for better understanding of the task.

4.1.1.1 Code explained for image extraction

There were 13 code segments to support the top-level code. The top-level code connects with other segments and provides the results. The basic tasks code segments were explained below.

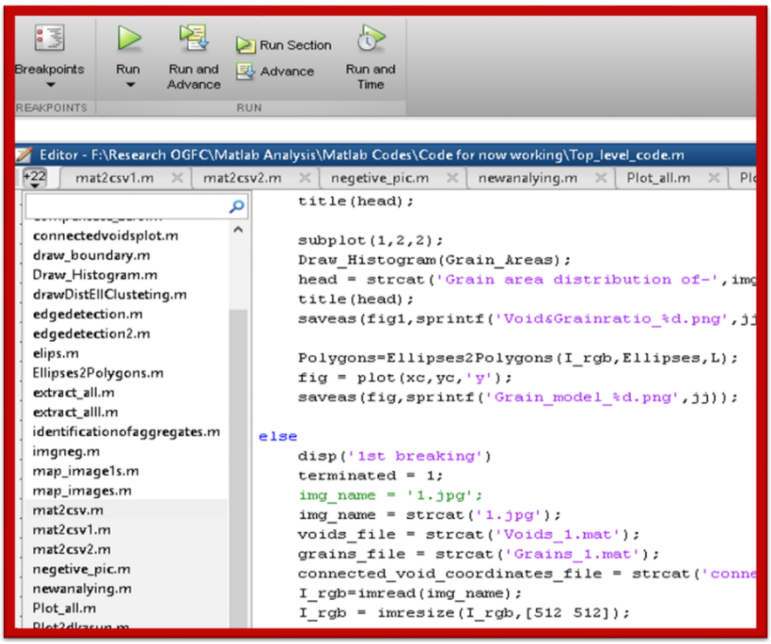

Figure 4.2: Interface of the MATLAB software with several code segments

Segments of image extraction code were shown in Figure 4.2. With the interface of the MATLAB. All the code segments used for this program is explained below.

4.1.1.1.1 Aggregate id

Reading image and identifying to its size and defining lengths and plots of the image ready to be analysed. Defining positioned, rows and columns of pixels. Introducing font sizes when to identify separate output images.

4.1.1.1.2 Compensesion zero

Algorithm to check each and every pixel as a pattern when running the other functions under top level code.

4.1.1.1.3 Crop image

Crop image as to a fair boundary

4.1.1.1.4 Draw boundary

Once the boundary is identified, this program segment supports drawing boundaries on all images.

4.1.1.1.5 Draw histogram

This is used to draw histograms of void aggregates details to understand the size variation. However, the same task was carried out by using excel algorithms later.

4.1.1.1.6 Edge detection

Detect all the boundaries of voids and aggregates and send the details of identified boundaries to top-level code.

4.1.1.1.7 Extract all

Defining smallest aggregate and void limits, enhancing accuracy of boundaries

4.1.1.1.8 Map images

Analysis of similar locations of 2D plans of different of cross sections.

4.1.1.1.9 Mat2csv

Convert created arrays and other information from .Mat files to .csv.

4.1.1.1.10 Top level code

Collaborate with all other function towards getting final outputs.

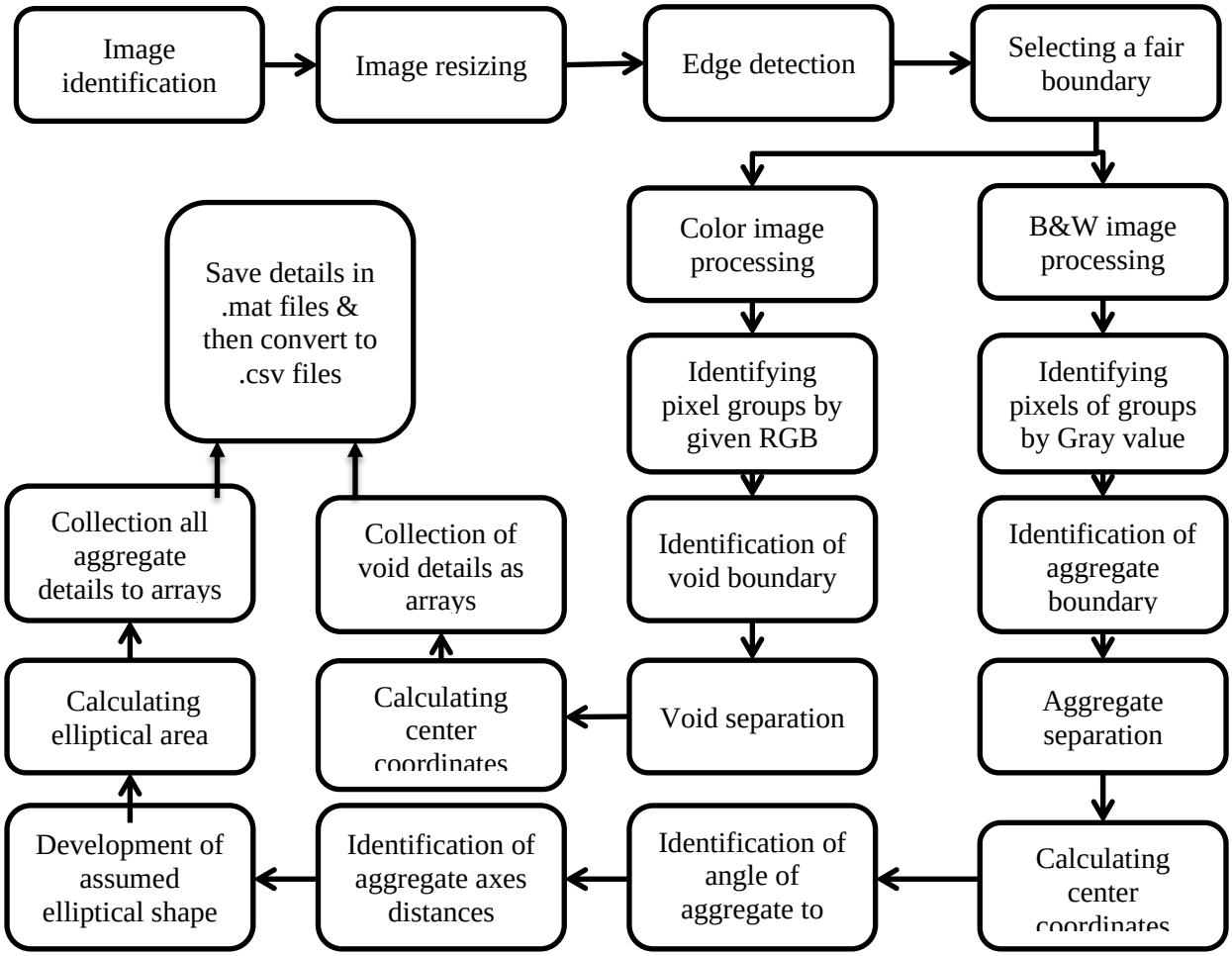

Figure 4.3: Functions of MATLAB algorithm for data extraction of cross-sectional images

4.1.1.2 Inputs

To analyse a single specimen, six cross-sectional images obtained were given as inputs to the program. Prior feeding the image details as inputs to the program, the cross sectional images were numbered from top to bottom as shown in Figure 4.4.

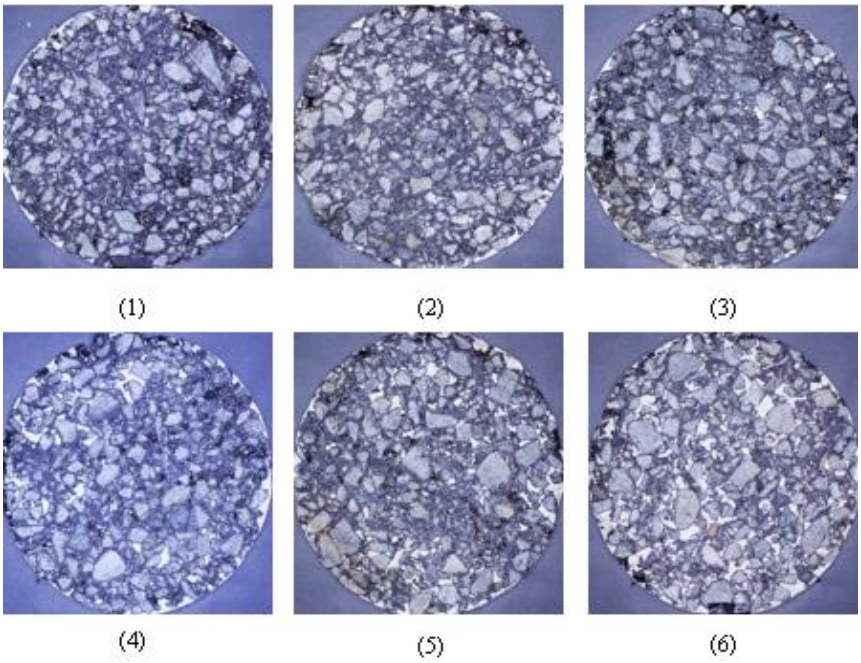

Figure 4.4: All input images of one specimen (images input per one execution)

4.1.1.3 Output

When all six images of one specimen were input to the MATLAB program, the following information was extracted per specimen.

4.1.1.3.1 Information as images

Figure 4.5 shows aggregates in white colour. These images were used to visually observe errors in identification of boundaries of aggregates compared to the original images. The aggregate centre identification and interconnected void area identification are indicated in Figure 4.6.

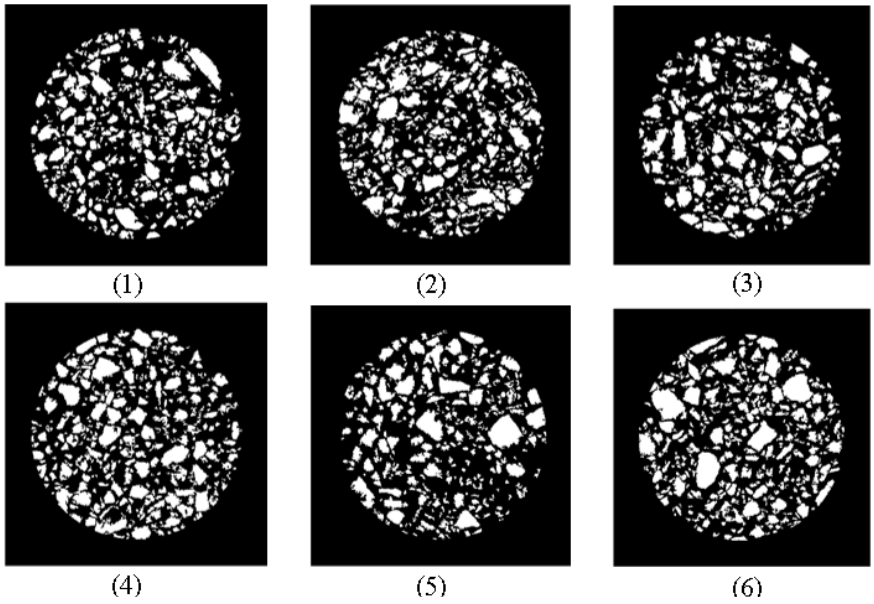

Figure 4.5: Black and white image of identified aggregates

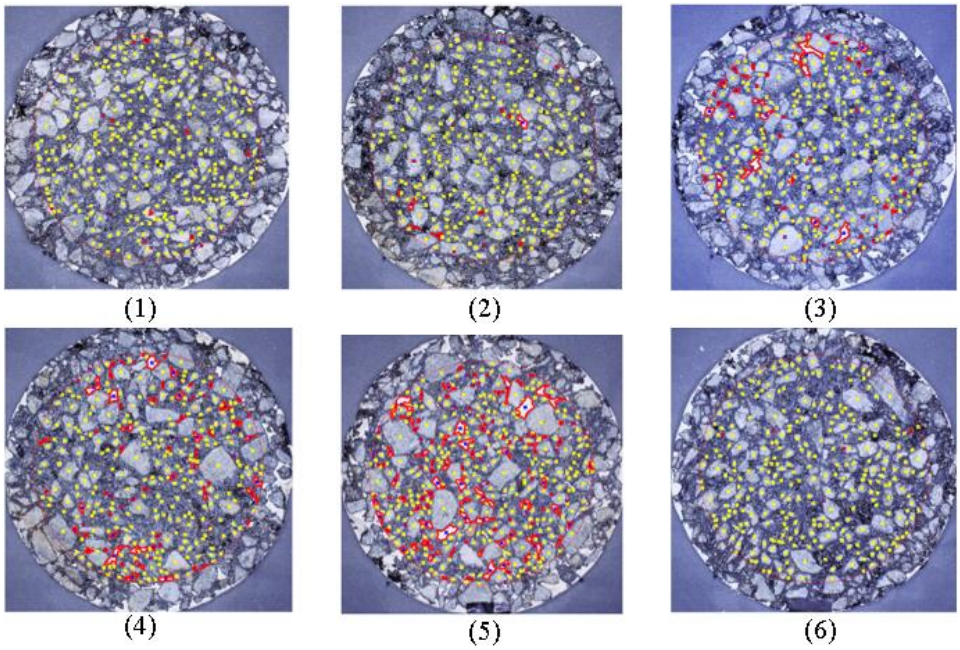

Figure 4.6: Voids and centres of aggregates and identified voids

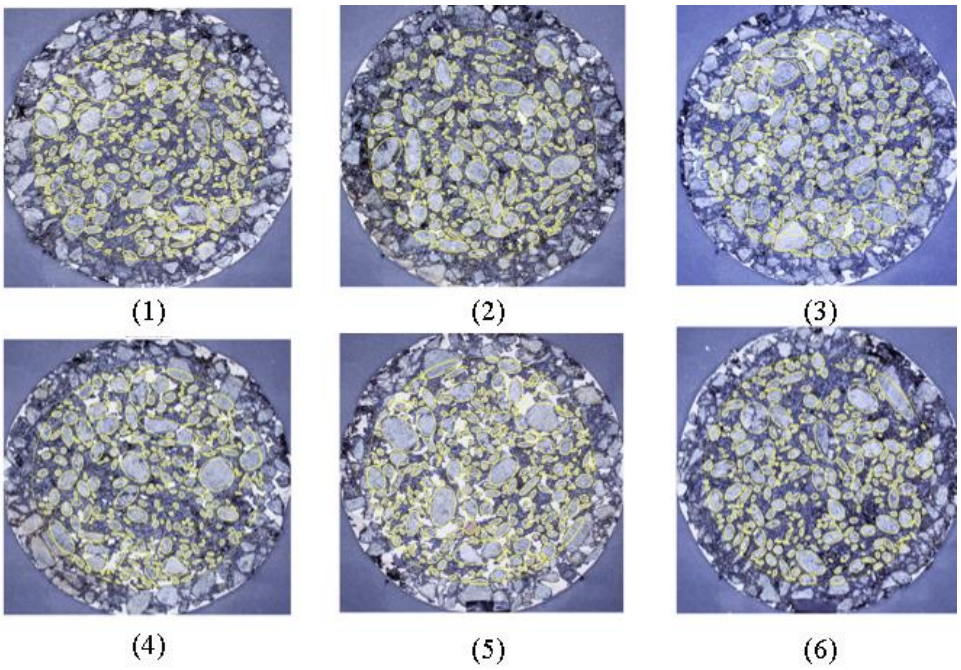

Figure 4.7: Aggregate shapes assumed as elliptical shapes marked on 2D images

The identification of aggregates and void arrangement was one of the major objectives of this study because; segregation and permeability characteristics of OGFC are dependent upon aggregate orientation and void arrangement. Therefore, the centre point identification of aggregates lead to assist segregation. Further, the aggregate shapes were mathematically approximated as elliptical shapes as shown in Figure 4.7. Several

information related to aggregate orientation angle, pixel area, etc. were collected using the elliptical shape approximation as described in the following chapter.

4.1.1.3.2 Information collected as number

According to the previous chapter, the elliptical approximation of aggregate shapes was used to determine a number of geometrical parameters of aggregates. The minor and major axis lengths stand for long and short direction lengths of the aggregate as shown in Figure 4.8. X and Y coordinates represents the coordinates of the centre of each aggregate in pixel lengths (Table 4.2). Another observation is the alignment of the aggregate w.r.t. the Y-axis of the global axis. The quantified angles are listed in Table 4.1.

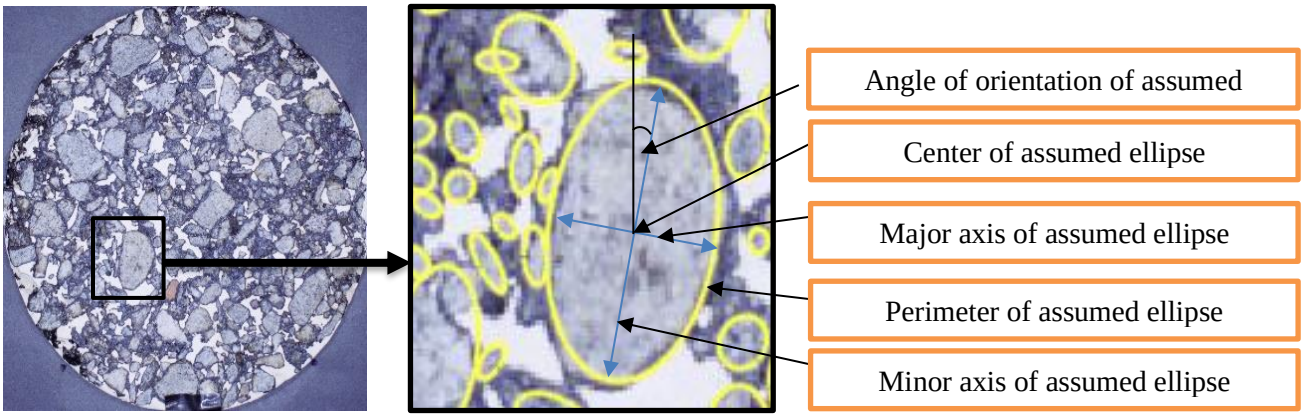

Figure 4.8: Collected details from projected elliptical shape

Table 4.1: Aggregate data collection

Minor axis length (mm)	Major axis length (mm)	X coordinate (Pixel length)	Y coordinate (Pixel length)	Orientation angle	Pixel area
1.5983	3.2980	307.93	371.07	112.59^0	15
2.0077	3.0427	320.40	118.13	44.81^0	15
1.5805	3.3280	389.80	143.00	145.57^0	15
2.1818	2.9806	403.73	263.87	22.849^0	15
1.9348	2.6897	412.53	136.07	151.68^0	15
1.8154	3.6322	430.07	354.20	100.75^0	15
1.7867	3.3642	105.69	373.44	179.67^0	16

Table 4.2: Void data collection

Void Number	X coordinate (Pixel length)	Y coordinate (Pixel length)	Area (Pixel)
1	59.281	250.13	64
2	76.216	216.75	1303
3	63.398	275.98	128
4	60.857	257.24	21
5	65.934	297.9	137

4.1.2 Extracting Delaunay distances

Delaunay distances are defined as centre-to-centre distances between adjacent aggregates. The average value of these distances can be taken as the distance between retaining on a particular sieve size. In this way, the distance identified can be used as a measurement of the distribution of aggregates w.r.t. different sieve sizes for a particular horizontal plane.

4.1.2.1 Codes explained

As shown in Figure 4.9, this algorithm consists with two code segments. One segment resizes he image to standard size and the other one creates the output image and the CSV file of the Delaunay triangle list.

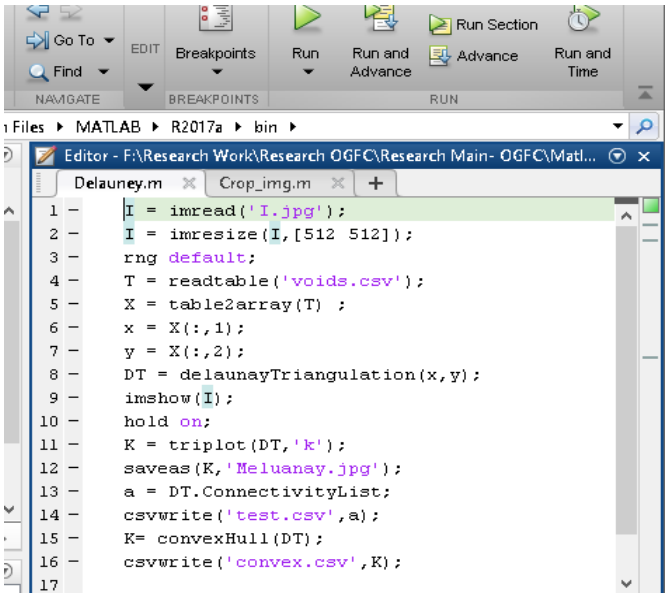

Figure 4.9 : Interface of the MATLAB software with the Delaunay distance algorithm

4.1.2.2 Inputs

The algorithm determining Delaunay distances requires an image and the corresponding centre coordinates of aggregates retaining on a particular sieve as input for the program to run. Figure 4.10 and Table 4.3 indicates sample versions of inputs as examples.

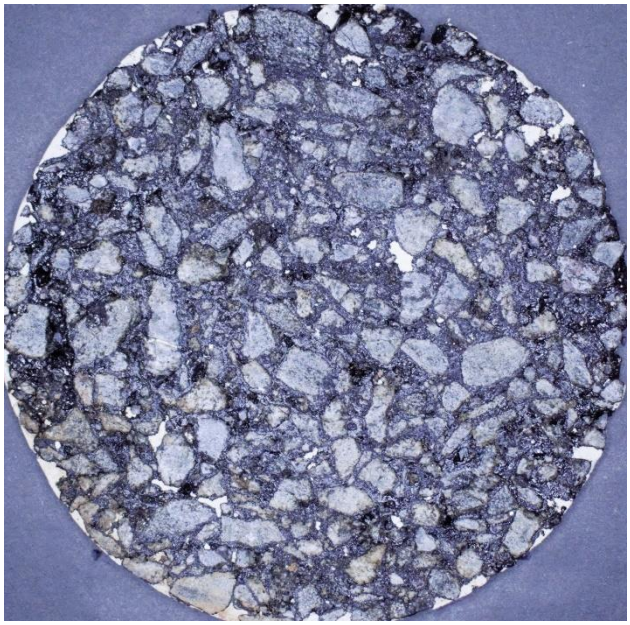

Figure 4.10 : Raw image prepared for processing

Table 4.3: Retaining aggregates of a sieve for the input of Delaunay algorithm

Corner No	X Coordinate	Y Coordinate
1	377.89	123.09
2	182.89	238.67
3	426.25	357.47
4	133.06	397.53
5	310.31	132.62
6	242.08	402.1
7	161.54	300.68
8	376.78	226.86
9	191.17	354.34
10	220.54	454.92

4.1.2.3 Outputs

The Delaunay distances extraction for selected sieve sizes was obtained as two outcomes from the program (Figure 4.11). Those were image outcomes and numerical outcomes. The following chapters elaborates sample versions of program outcomes in detail.

4.1.2.3.1 Information as images

Figure shows the distances between centres of the aggregates retaining on 4.75 mm sieve. These output images support the visual observation of the distribution of aggregates of same sieve size.

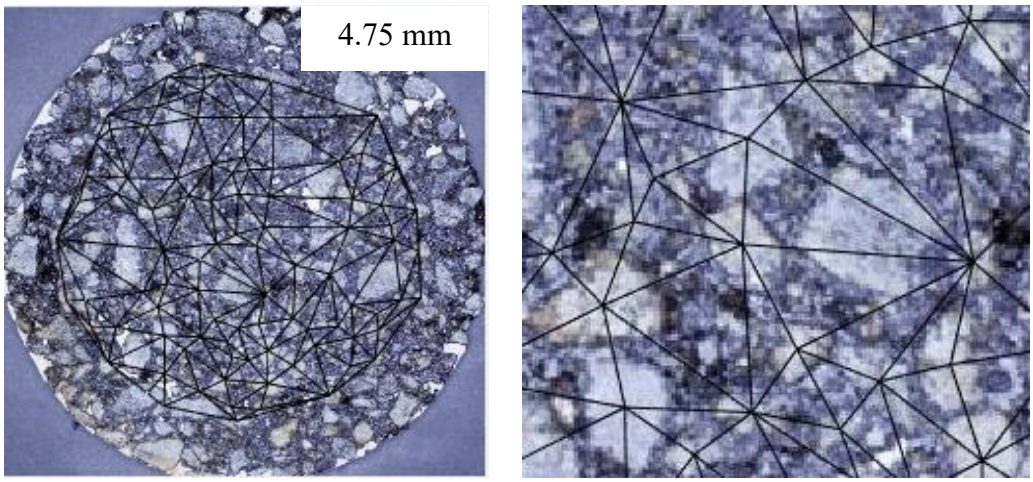

Figure 4.11: Output image of Delaunay distance algorithm

4.1.2.3.1 Numerical information

The numerical outputs of the program were Delaunay triangles CSV file along with Convex CSV file including the information shown in Table 4.4. This information were used to calculate distances between aggregates (Delaunay distances) with the aid of the coordinate file of the corresponding sieve size.

Table 4.4: Corner aggregates of (a) Convex and (b) Delaunay triangles

Corners of polygon
3
13
15
10
51
70
69
50
3

(a)

Corner 01	Corner 02	Corner 03
110	42	3
78	27	66
39	85	50
82	33	57
102	36	80
98	5	53
11	22	100
24	23	20
93	36	37
93	25	36

(b)

4.2 Processing of MATLAB outputs

The data extracted were processed to analyse and obtain several objectives. There were number of information created for purposes mentioned below.

4.2.1 Calculation of minimum size of area retaining value for aggregate segments

To carry out this, data gathered from three-control specimen were used. All the aggregate areas of all six cross sections of one specimen was collected to one excel sheet. All the details were sorted by ascending order using the area of a cross section of aggregates. The cumulative area, the summation of areas at each row was calculated considering from the top to the selected row. Total of all areas were divided according to the percentages of gradations. This analysis, the smallest aggregate size analysed by the image analysis was limited to 1.18 retaining aggregates by the performance of the code data and the computer used. The corresponding area values for every retaining sieve values were calculated by the use of this method. Finally, all three-control specimen were subjected to the same procedure and the average area retaining value of each sieve was taken as the size of the minimum aggregate area retaining on a particular sieve. These calculated area values are similar to the sieve sizes. As the aggregate weight retained on a sieve is used to calculate the percent retaining on a sieve, the minimum aggregate area retaining on a sieve can be used to analyse the percentage retaining corresponding to the sieve size using image processing.

4.2.2 Arrangement and processing of data for visualization inputs

The interconnected void network model was created on excel platform as shown in Figure 4.12.

4.2.3 Development of interconnected void models

X-axis	Y-axis	Size	Z-axis	Layer	Grains Voids	Information	Number
216	65	49	6	Layer01	Voids	6	A1
243	76	31	6	Layer01	Voids	6	A2
266	77	21	6	Layer01	Voids	6	A3
229	78	08	6	Layer01	Voids	6	A4
347	78	32	6	Layer01	Voids	6	A5
327	91	78	6	Layer01	Voids	6	A6
250	92	19	6	Layer01	Voids	6	A7
240	95	15	6	Layer01	Voids	6	A8
196	100	168	6	Layer01	Voids	6	A9
302	100	297	6	Layer01	Voids	6	A10
287	108	85	6	Layer01	Voids	6	A11
147	115	58	6	Layer01	Voids	6	A12

Figure 4.12 : Interface of the algorithm developed to obtain interconnectivity of voids

4.2.4 Distance between aggregates

As a result of MATLAB program for Delaunay distances, two .csv files were obtained. With the aid of the coordinates of aggregates file and the above-mentioned two .csv filed, distances of all the legs combining all aggregates were calculated. The average of the distances calculated was taken as distance between aggregates. These distances were found for each aggregate retaining on a sieve.

4.3 3D Visualization of data

3D visualizations were created by the use of Python programming language. These algorithms were built using Anaconda Navigator- Jupytor notebook (web-based, interactive computing notebook environment) with plotly library (online data analytics and visualization tool). Two programs were building on Python to obtain two different visualization outputs such as void and aggregate plotting in 3D space and plotting of predicted interconnected void networks.

5. RESULTS AND DISCUSSION

This chapter discusses the experimental and software simulation results leading to obtain the aims and objectives of the study. Initially, the experimental data is presented to understand the behaviour of the selected three types of OGFC in terms of permeability and durability. Then, the parameters of the image analysis is discussed in the means of pixel areas and mathematical outcomes. The 3D void/aggregate arrangement and the interconnected void network were developed based on assumptions.

5.1. Experimental test results comparison

5.1.1 Permeability test data

The permeability measurements were collected from six specimens for different gradations. The specimens were 60 mm in height. When considering the permeability values in Table 5.1, C specimens have a higher average permeability value and A specimens have the lowest value. However, when comparing the individual permeability values of B specimens, the permeability is much closer to A specimens.

Table 5.1: Experimental results of permeability test

Gradation	k1 (mm/s	k2 (mm/s)	k3 (mm/s)	k4 (mm/s)	k5 (mm/s)	k6 (mm/s)	k(mm/s)	Standard Dev.
A	0.75	0.74	0.84	0.83	0.94	0.77	0.81	0.08
B	1.07	1.04	1.02	1.1	1.02	0.98	1.04	0.04
C	2.58	2.47	2.65	2.61	2.38	2.54	2.54	0.10

5.1.2 Durability test data

The Los Angeles Abrasion test was conducted to determine the durability of OGFC specimens. Six number of specimens were used to check the durability of different gradations. The specimens were 150 mm in height. When considering the durability measurements in Table 5.2, C specimens have the lowest average durability and A specimens have the highest durability. However, when comparing the individual durability values of A and B specimens, abrasion losses were approximately similar in most of the specimens. Further, the standard deviation of abrasion loss of all A, Band C specimens were around 1%.

Table 5.2: Experimental results of durability test

Gradation	Sample 1 (%)	Sample 2 (%)	Sample 3 (%)	Sample 4 (%)	Sample 5 (%)	Sample 6 (%)	Avg. Cantabro Loss (%)	Standard Deviation
A	8.09	6.43	6.73	9.089	6.829	6.081	7.21	1.15
B	10.74	9.20	8.97	11.22	7.684	9.516	9.56	1.28
C	11.45	12.82	13.00	11.599	13.44	12.014	12.39	0.81

5.1.3 Relationships among air voids, durability and permeability

The variation of number of interconnected voids and the total area of interconnected voids against the depth of the OGFC specimen is indicated in Figure 5.1. When comparing the two graphs, it is evident that the inter connectivity becomes lower along with the depth of the specimen.

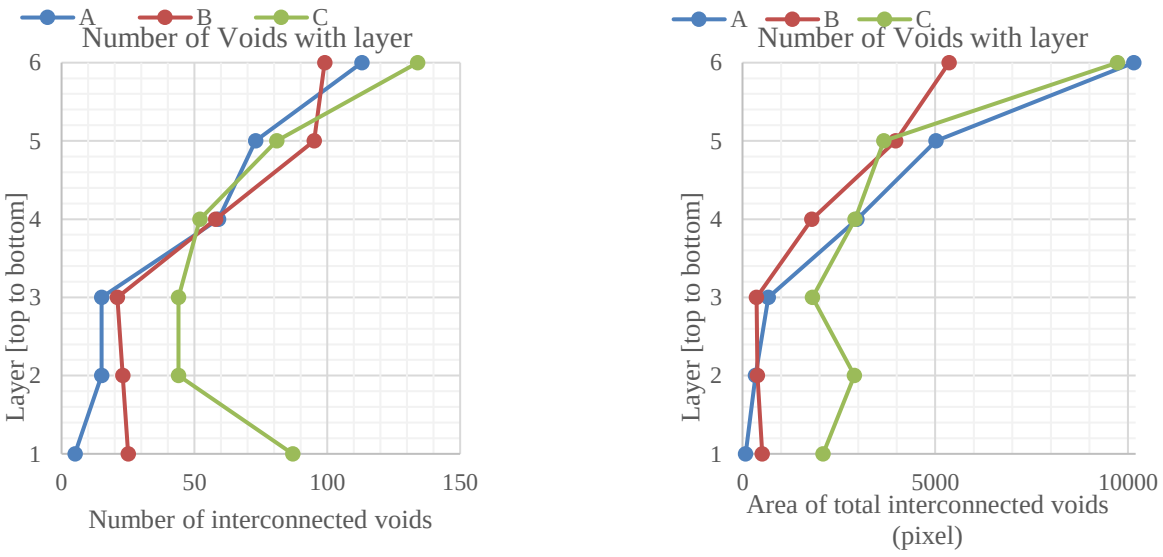

(a) (b)

Figure 5.1 : Change of (a) number of interconnected voids and (b) area of interconnected voids with the depth

The void quantification was carried out using areas due to the image data obtained are usually 2-dimentional. However, calculating volumes using only six image data per specimen could not provide valid information on volumes due to lack of data on voids. Therefore, this study was focused on comparing 2D and 3D data to find relationships of durability and permeability.

5.1.4 Total voids Vs permeability

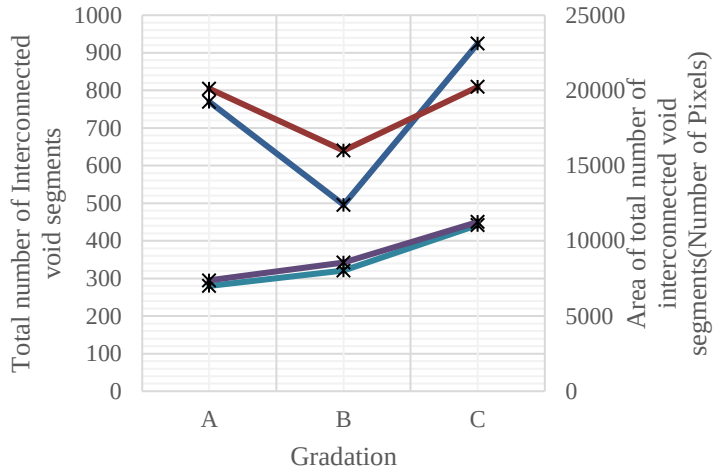

Figure 5.2 : Total and area of voids of three different gradations

As shown in Figure 5.2, when the total number of interconnected void segments showed a slight variation, total area of interconnected void segments showed a higher variation. Therefore, the total number of interconnected voids segements were graphed against the permeability experimental results as shown the Figure 5.3. This provides a slightly linear relationship and the curve does not move through the origin of the graph. Further, this concludes that the total area of inerconnected voids do not bahave linearly with permeability.

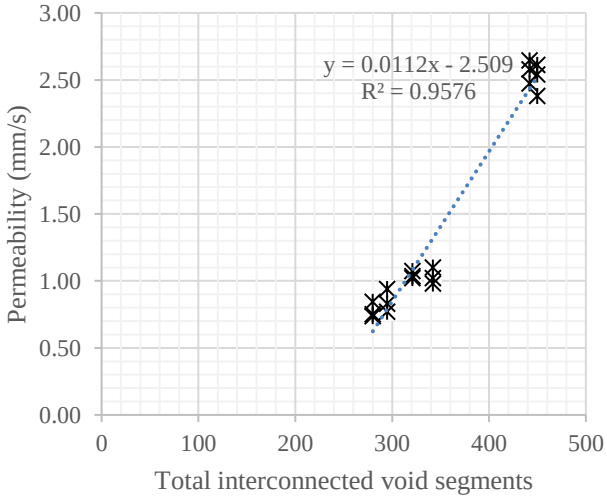

Figure 5.3 : Relationship between permeability and total interconnected void segments

5.2 3D visualization of data

Mathematically processed data from raw images were imported on software programs for 3D visualization. This 3D illustration supported to visually observe the internal void network, aggregate packing, number of voids variation through the depth of the OGFC specimens more meaningfully.

5.2.1 Interconnected Void Distribution

Figure 5.4 shows the 3D illustration of identified void segment arrangement and void sizes of three gradations. All six image per specimen was used to model the void arrangement of OGFC. These models can be checked in any angle by rotating and zooming for visual observations.

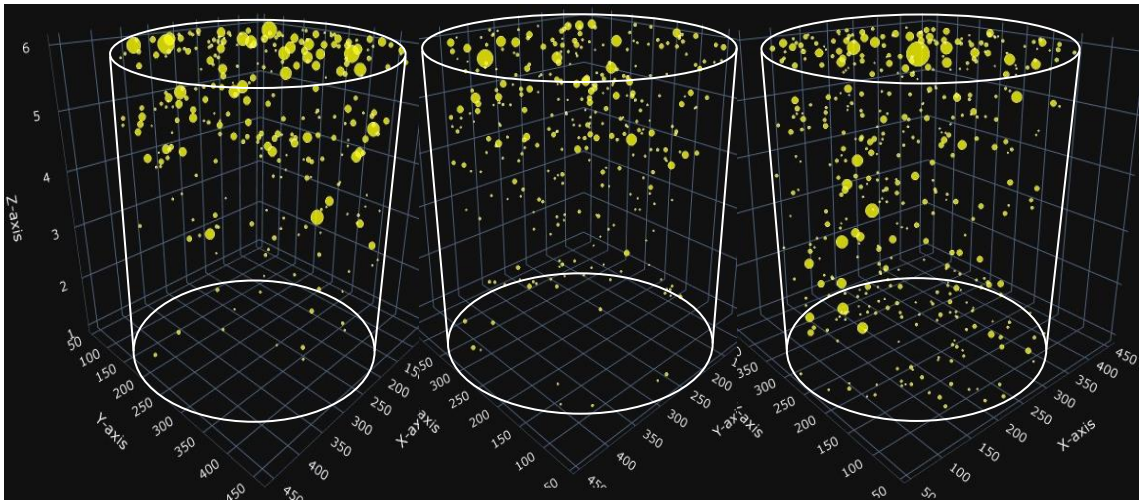

(a) (b) (c)

Figure 5.4 : 3D illustration of identified void segment arrangement and void sizes of (a) Gradation A, (b) Gradation B and (c) Gradation C

5.2.2 Aggregate distribution obtained by image processing

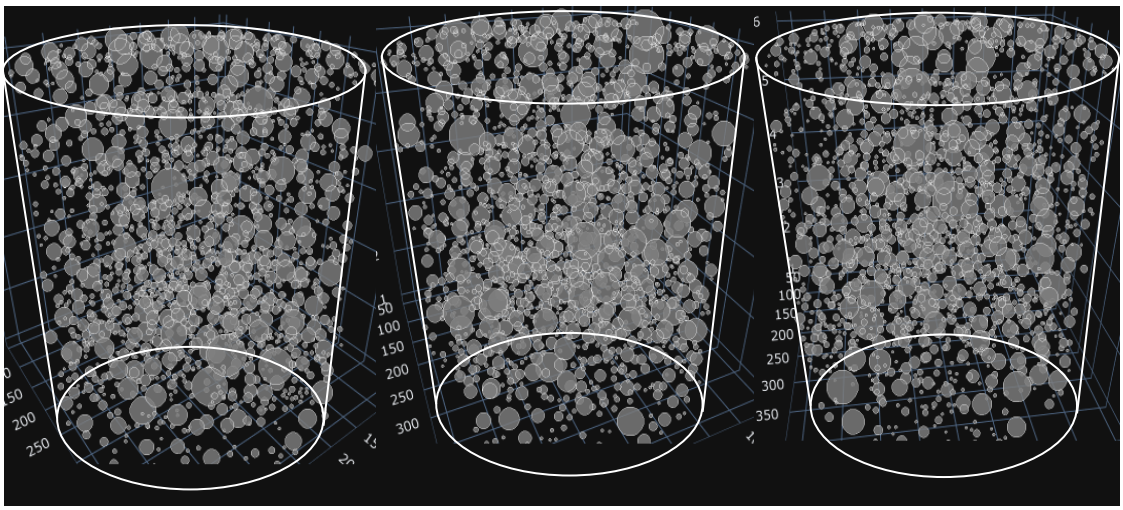

(a) (b) (c)

Figure 5.5 : 3D illustration of identified aggregate segments coordinates and sizes of (a) Gradation A, (b) Gradation B and (c) Gradation C

Notebook 6.0.3 which is a wab-based interactive computing notebook environment. ‘Scatter_3D’ was the main function used for this illustration on Python plotly. According to Figure 5.5, all the observed aggregate arragements in OGFC specimen can be observed. However, these figure visually are the same, major segregations or void areas can be observed.

5.2.3 Simulated interconnected void networks

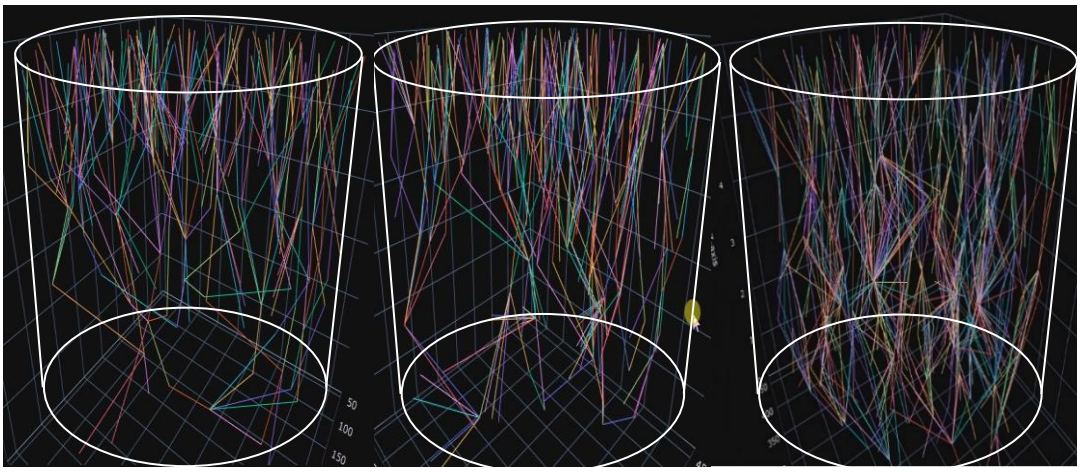

(a) (b) (c)

Figure 5.6 : Prediction model 01 developed for (a) Gradation A specimen, (b) Gradation B specimen and (c) Gradation C specimen

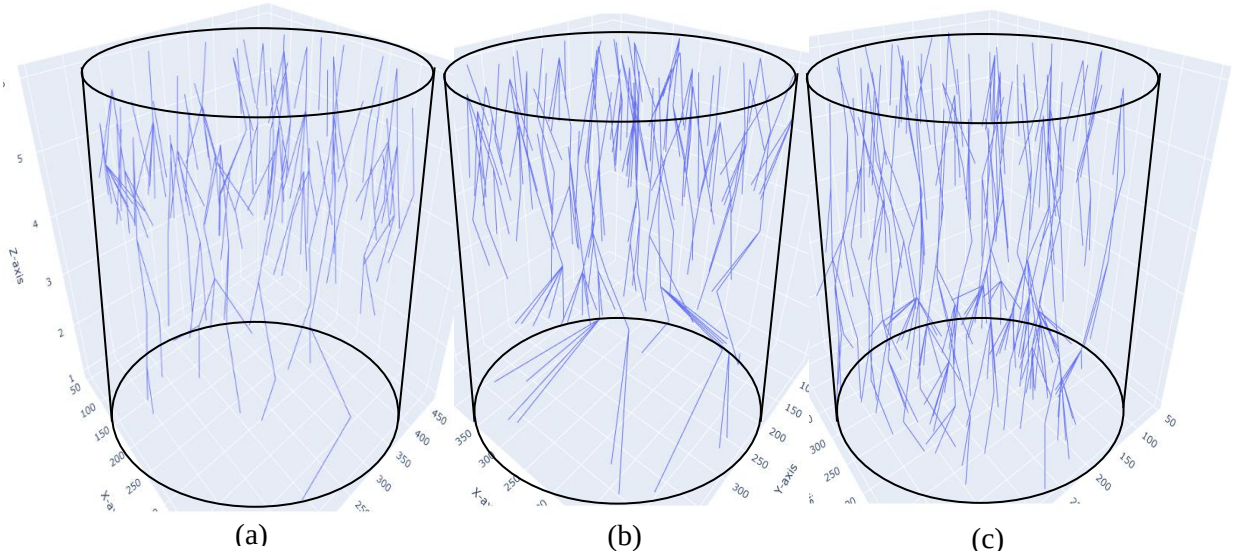

Figure 5.7 Prediction model 01 developed for (a) Gradation A specimen, (b) Gradation B specimen and (c) Gradation C specimen

3D illustrations of Figure 5.6 and Figure 5.7 were built in plotly mainly using line_3d function. Using the void segements data obtain from the images, two algorithms were developed on excel how the void interconnectivity can take place. Prediction model 01 and 02 showed different arrangements due to the differernt assumptions made in their algorithms. However, it can be easily observed that the interconnectivity network is higher from gradation C specimen to gradation A specimen for both models. Although, the visual observations were clear to compare the interconnectivity of the specimens with the other specimens, a method of quantification was required.

A parameter was difined using the interconnectivity models to release a value to be compared with its permeability. One path connecting from one layer to next consecative layer was difined as one path segment. Therefore, the number of path segments influencing the interconnectivity from top to bottom were calculated and named as the path index. The path indexes were counted using the same algorithm developed in excel.

5.3 Aggregate distribution analysis

An aggregate as same as a volumetric detail of an aggregate in its physical stage. Although, the sieve size provides an area to pass aggregates through the sieve, the sieve size is generally mentioned as width of an orifice of the sieve. In order to separately identify retaining masses using image analysis, a pixel area was determined as the minimum aggregate area retaining on a particular sieve. Calculated area using one orifice of a sieve to obtain the minimum area of aggregate retaining on the sieve may not be accurate due to the difference between the areas of cut surface of an aggregate in the cross section by image processing, and surface with the maximum cross-sectional area parallel to the sieve of the aggregate when it is passing through the sieve, may be different as shown in the Figure 5.8.

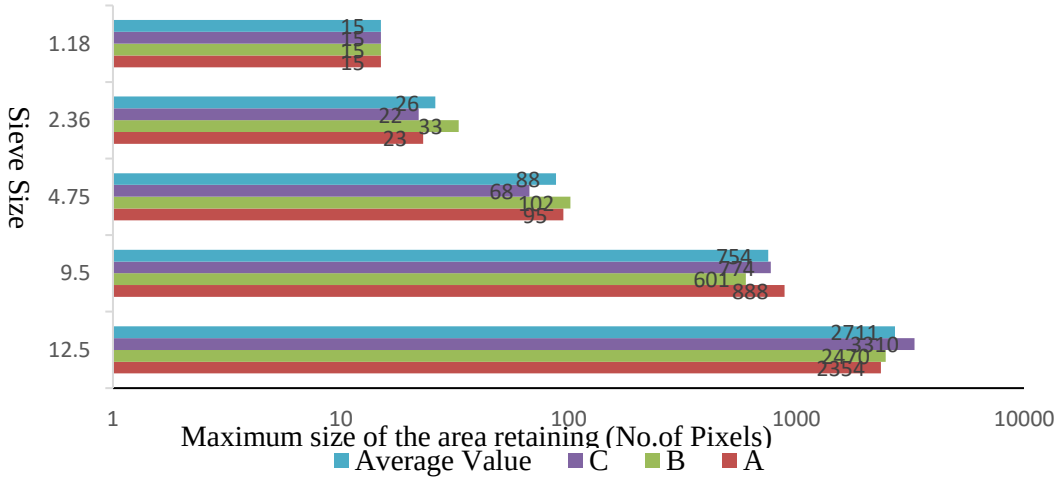

Figure 5.8: The minimum aggregate area retaining on each sieve of each sample in pixels by Area Approximation Method

In order to obtain the minimum aggregate area retaining on a sieve, Area Approximation Method (AAM) was developed using the cross-sectional data of aggregates obtained by image processing analysis and experimental gradation proportions. These pixel area data from image processing were arranged in descending order and cumulative area values were calculated for each aggregate size. Then, the cumulative values were proportionately divided according to the original gradation proportions and the minimum aggregate area retaining on a sieve was obtained for each samples separately as shown in Figure 5.8. Considering all the samples, the minimum aggregate area retaining on a sieve was calculated as a mean value for each sieve.

Once the minimum aggregate area retaining on sieves were calculated, the original gradations and the gradations obtained from image analysis were compared as shown

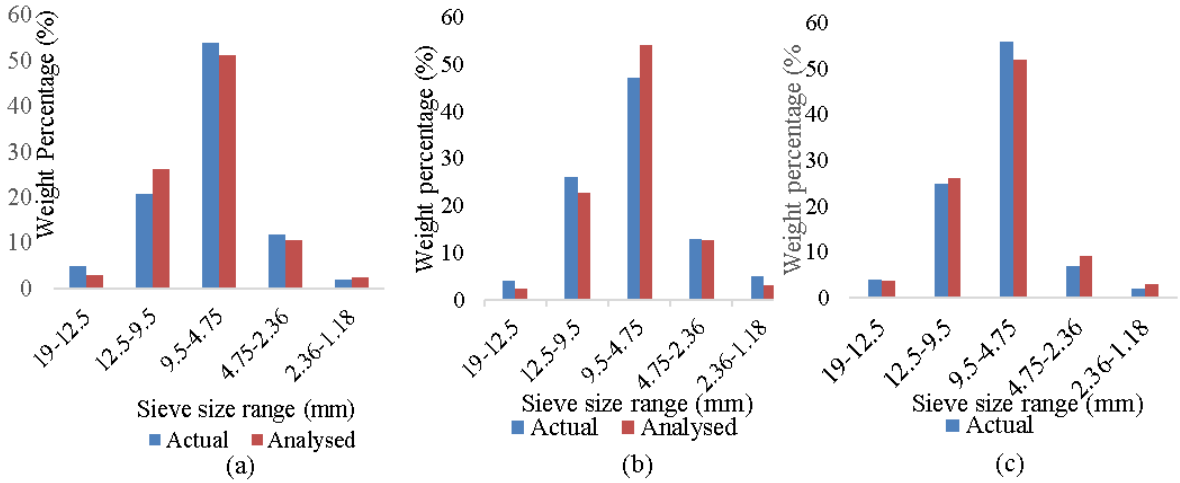

Figure 5.9: Validation of the area approximation method by comparison of experimental retained aggregate weights and weights calculated based on the AAM; (a) Sample A, (b) Sample B, and (c) Sample C percentages

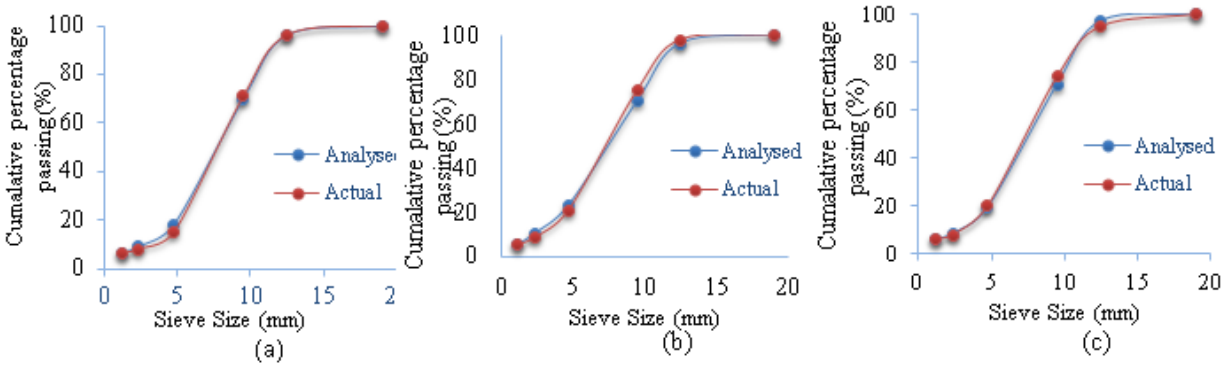

Figure 5.10: Comparison between Maximum area of aggregate passing through the sieve sizes based on AAM and original sieve sizes for (a) Sample A, (b) Sample B, and (c) Sample C.

5.4 Vertical segregation analysis

Table 5.3: Sieve analysis using area measurements in layers.

Layer No	Sieve Size(mm) - minimum aggregate area retaining on a sieve									
A	1.18-15		2.36-26		4.75-88		9.5-754		12.5-2711	
	Number	Area	Number	Area	Number	Area	Number	Area	Number	Area
1	61.00	1204.00	123.00	6216.00	98.00	24644.00	8.00	11241.00	2.00	6170.00
2	56.00	1088.00	110.00	5370.00	82.00	21394.00	9.00	11279.00	1.00	2797.00
3	69.00	1333.00	100.00	4975.00	110.00	31624.00	10.00	11622.00	0.00	0.00
4	89.00	1689.00	78.00	3767.00	94.00	26470.00	11.00	12132.00	0.00	0.00
5	71.00	1381.00	123.00	6132.00	95.00	23440.00	12.00	15103.00	0.00	0.00
6	62.00	1248.00	110.00	5560.00	103.00	25814.00	9.00	10840.00	0.00	0.00
CV/M	15.57 / 1323.83		16.87 / 5336.67		13.59 / 25564.33		12.99 / 12036.17			
L_i	[926.68	1720.98]	[3735.67	6937.67]	[17895.03	33233.63]	[8425.32	15647.02]		
B	1.18-15		2.36-26		4.75-88		9.5-754		12.5-2711	
	Number	Area	Number	Area	Number	Area	Number	Area	Number	Area
1	52.00	1053.00	82.00	3984.00	110.00	32550.00	8.00	8066.00	0.00	0.00
2	77.00	1559.00	104.00	5174.00	98.00	26074.00	5.00	6182.00	0.00	0.00
3	71.00	1383.00	95.00	4653.00	78.00	20341.00	6.00	7917.00	0.00	0.00
4	59.00	1202.00	100.00	4751.00	106.00	25386.00	5.00	5985.00	0.00	0.00
5	91.00	1796.00	148.00	**7485.00**	105.00	25618.00	2.00	**2391.00**	0.00	0.00
6	82.00	1650.00	102.00	5221.00	87.00	22567.00	12.00	**14644.00**	1.00	3242.00
CV/M	19.50 / 1440.50		**23.03** / 5211.33		16.24 / 25422.67		**53.66** / 7530.83			
L_i	[1008.35	1872.65]	[3647.93	6774.73]	[17795.87	33049.47]	[5271.58	9790.08]		
C	1.18-15		2.36-26		4.75-88		9.5-754		12.5-2711	
	Number	Area	Number	Area	Number	Area	Number	Area	Number	Area
1.0	75.00	1487.00	92.00	4774.00	84.00	23757.00	13.00	**17604.00**	0.00	0.00
2.0	99.00	1889.00	112.00	5613.00	101.00	22431.00	9.00	9569.00	1.00	3666.00
3.0	62.00	1218.00	82.00	3974.00	124.00	33034.00	9.00	9559.00	2.00	7535.00
4.0	62.00	1273.00	66.00	3497.00	112.00	30374.00	12.00	12322.00	0.00	0.00
5.0	64.00	1244.00	102.00	4876.00	95.00	25146.00	9.00	12465.00	0.00	0.00
6.0	96.00	1861.00	100.00	4730.00	96.00	22141.00	14.00	**17347.00**	0.00	0.00
CV/M	**20.68** / 1495.33		16.22 / 4577.33		17.26 / 26147.17		**27.29** / 13144.33			
L_i	[1046.73	1943.93]	[3204.13	5950.53]	[18303.02	33991.32]	[9201.03	17087.63]		

Number - Number of aggregates identified in a cross section as retaining on a particular sieve
Area - Total area of aggregates identified as retaining on a particular sieve
CV - Coefficient of variation
M – Mean area of aggregates identified as retaining on a particular sieve
L_i- Allowable region where an area of a particular sieve can remain without segregation - [lower limit upper limit]

Six cross sections obtained from top to bottom of the specimen can be used to understand the grading with the depth of the specimen. Layers of specimen were marked from layer 01 to layer 06 as from top to bottom. The gradations at different layers are shown in Figure 5.11.

Aggregate weight proportions are similar to the total area of aggregates identified as retaining on a particular sieve and the number of aggregates identified is similar to the aggregates on a particular cross-sectional plane. As the 'Number' of aggregates retaining on 12.5 mm sieve were low in all specimen types, the percentages may not be highly reliable (Table 5.3). However, greater gradation deviations at each layer can be recognized using this method. The number of aggregates retaining on 12.5 mm sieve to cast one specimen is around 10 to 15. Even though, the number of cross sections were six and the possibility of identifying a 12.5 mm retaining aggregate from the image analysis is low, identifying retaining percentages on sieve sizes less than 12.5 mm is possible.

Coefficient of variation (CV) = Mean / Standard Deviation

L_i = [lower limit upper limit] ≡ [(M – 30%M) (M + 30%M)]

If the area value of any layer lies out of the L_i limit, that particular layer may consider as segregated by this analysis. Further, when the area values of layers remained out of the L_i limit, all the CV values of sieves were more than 20%. Therefore, 5th and 6th layer of the specimen B and 1st and 6th layer of the specimen C were segregated according to the analysis given in Table 5.3.

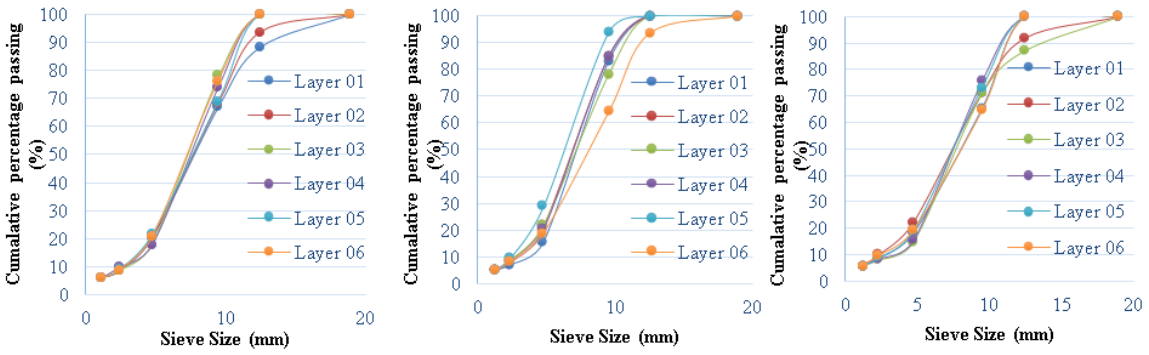

Figure 5.11 : Sieve analysis by DIP of different layers of (a) Sample A, (b) Sample B, and Sample (c)

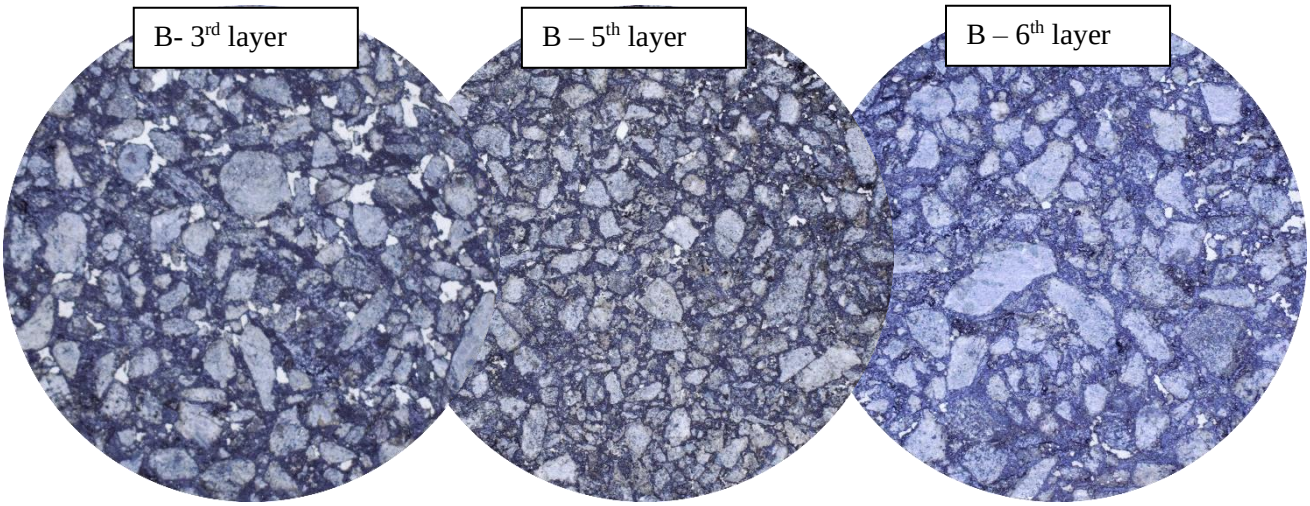

Figure 5.12 : Raw images of selected cross sections for validation

An example can be given from the stated three types of OGFC samples. When the cross-sectional gradations are considered, cross-sections of specimen B shows higher deviations than the cross sections of the other specimens (Figure 5.11). When considering specimen B, it can be observed that the layer 05 and the layer 06 were deviated from the other layers as shown in Figure 5.4.1(b). 3rd layer of specimen B approximately coincides with the original grading of the sample and the original image of 3rd layer is shown in Figure 5.12. According to Figure 5.4.2, compared to the actual cross sections of the 3rd layer of the specimen B, 5th layer contains higher fine proportion and lower coarse proportion while 6th layer contains lower fine proportion and higher coarse proportion. This visual observation complies with the sieve analysis by DIP shown in Figure 5.11 (b) as well. Therefore, it is clear that it can be quantified the variations as numerical figures using the proposed DIP method. Further, this method enables quantifying segregations, deviations in gradations and unnecessary voids.

5.5 Horizontal segregation

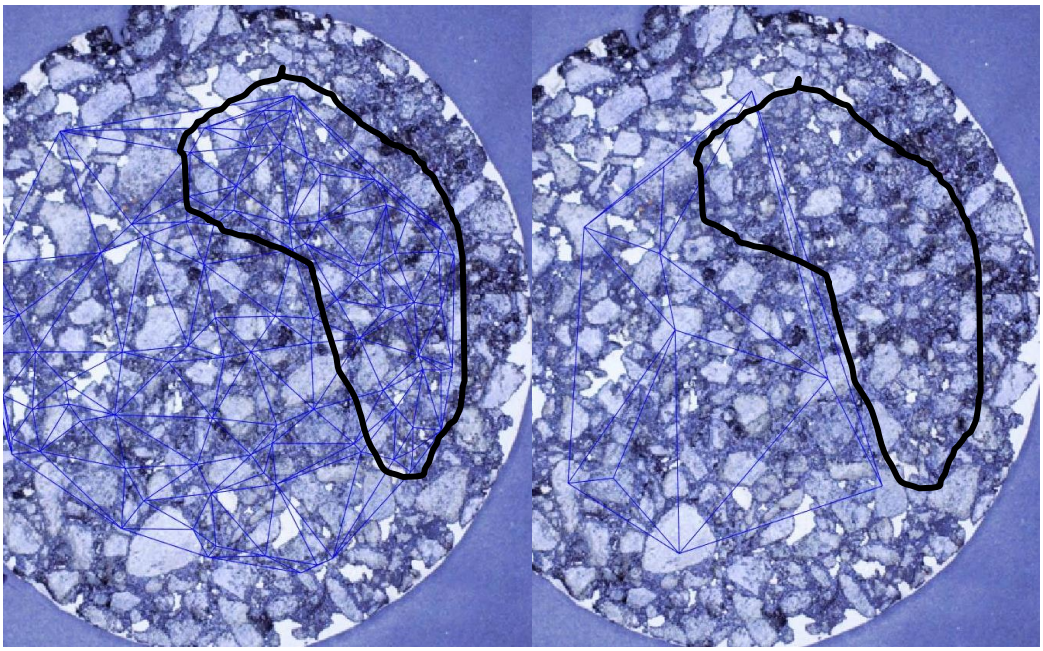

Figure 5.13: Cross section of a horizontally segregated area for (a) 2.36 mm and (b) 9.5 mm retaining aggregates

Distances obtained from Delaunay triangles can be used to identify segregation in the horizontal plane. Figure 5.13 provides evidences for such scenario. According to the images given under Figure 5.13, 2.36 mm retaining aggregates are highly available within the black colour outlined area while 9.5 mm retaining aggregates are unavailable in the same area. This observation can be visually identified when the Delaunay triangles are drawn as shown in Figure 5.13. Further, this method can be enhanced to automatically identify the internal horizontal segregations at any depth. Although, the parameters of Delaunay triangles such as distances and angles can be used to quantify these segregations precisely, the output of the algorithm should be developed to indicate the segregation in compliance with how human identifies.

Table 5.4: Distance between aggregate analyzed using Delaunay triangles

		Distance between aggregates							
	Sieve size	**1.18**		**2.36**		**4.75**		**9.50**	
	Layer	**AVG**	**STDV**	**AVG**	**STDV**	**AVG**	**STDV**	**AVG**	**STDV**
A	**1**	53.24	29.95	39.10	23.48	41.13	18.13	142.55	45.80
	2	59.39	38.72	41.07	24.37	47.51	22.58	142.55	59.56
	3	53.24	26.78	42.47	24.93	41.13	16.87	137.77	67.05
	4	44.61	26.21	49.49	26.55	44.33	20.43	126.07	49.31
	5	52.36	32.20	40.42	22.32	43.57	21.57	120.25	50.96
	6	57.14	29.98	41.91	26.22	42.52	19.17	132.18	53.77
	Average	**53.33**	**30.64**	**42.41**	**24.65**	**43.37**	**19.79**	**133.56**	**54.41**
B	**1**	60.09	33.07	46.78	28.23	40.77	17.74	119.85	49.91
	2	48.06	29.76	41.05	23.05	43.89	20.03	156.20	52.72
	3	48.94	27.07	44.78	24.05	48.61	21.50	194.18	64.30
	4	57.29	31.09	51.41	24.00	50.20	19.48		
	5	45.61	27.43	35.73	22.40	41.91	20.13		
	6	48.26	28.06	43.12	23.03	46.76	24.45	115.52	48.72
	Average	**51.38**	**29.41**	**43.81**	**24.13**	**45.36**	**20.56**	**146.44**	**53.91**
C	**1**	49.61	29.63	45.24	26.54	46.22	23.00	88.71	40.05
	2	54.20	22.24	41.47	23.31	43.42	20.79	118.98	62.80
	3	53.97	33.77	48.62	24.84	38.69	16.75	113.97	45.41
	4	55.48	27.82	52.13	30.37	41.10	20.52	132.57	78.02
	5	55.06	32.04	42.89	25.00	44.63	22.54	143.40	73.11
	6	50.12	26.55	42.12	25.90	43.29	19.38	107.13	61.54
	Average	**53.07**	**28.68**	**45.41**	**25.99**	**42.89**	**20.50**	**117.46**	**60.16**

AVG – Average distance between aggregates of a cross section
STDV – Standard deviation of distance between aggregates of a cross section

Table 5.4 shows the average distances between aggregates retaining on a different sieve size. As explained previously, these values can be useful for the development of the quantification of horizontal segregation using Delaunay triangles. When the size of the aggregates gets higher, it can be noted that the distance between aggregates is reduced and vice-versa.

Table 5.5 indicates a method to identify the segregation location of a selected cross section. The segregation identification is important at this design stage because, if same size aggregates get crowded closely, the permeability and durability would be adversely affected. Therefore, considering the possibility of having partial segregations on a selected cross section of a specimen, the following method was developed to predict the segregation.

The segregation was defined in the computer program by the closely spacing of same size aggregates. When identifying the region of area of segregation on a selected plane, the following steps were followed.

1. Each quarter of the cross section was first checked for number of aggregates available in the considering quarter.
2. The percentage of same size aggregates in each quarter was calculated. When comparing the visual inspection of segregation of cross sections and Delaunay triangles, 10% was selected as the lower boundary for the segregation for 1.18 mm, 2.36 mm and 4.75 mm. 9.5 mm and 12.5 mm aggregates were not available on specimen layers in larger quantities (Table 5.4). Therefore, segregation was supported by 9.5 mm and 12.5 mm aggregate sizes.
3. Then the percentage of aggregates in halves of a considered plane area were checked in both perpendicular directions. This was done to identify the aggregate crowded area regions, which were not checked in previous quarter checking. The lower boundary of the segregation for 1.18 mm, 2.36 mm and 4.75 mm aggregates was 20%.
4. The segregation at the centre of the plane considered was quantified by checking the aggregate numbers at the circular area. The inner circular area was equal to a half of the total area of the plane considered. The segregation lower boundary for this check was 20%.

The aforementioned procedure and lower boundaries of aggregate availability per area were selected based on the observations from this study. The most important point is that, when developing this study to check different field related asphalt specimen observation, Engineers can change the numerical parameters based on the experimental specimen data. As an example, based on the project, the boundaries of segregation can be changed as according to the requirements of the project.

Further, this analysis cannot carry out using the traditional methods used so far. Therefore, for further development of OGFC, these methods can be carried out to enhance the construction practices as well.

Table 5.5: Horizontal segregate analysis of sample from specimen A

Sieve size	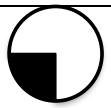	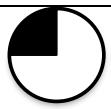	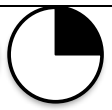	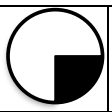	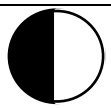	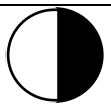	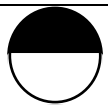			
	Quarter 01	Quarter 02	Quarter 03	Quarter 04	Half/Half 01	Half/Half 02	Half/Half 01A	Half/Half 02A	Circle inside	Circle outside
1.18	18.0	27.9	26.2	27.9	45.9	54.1	44.3	55.7	45.9	54.1
2.36	23.6	25.2	26.0	25.2	48.8	51.2	49.6	50.4	55.3	44.7
4.75	16.3	26.5	25.5	31.6	42.9	57.1	41.8	58.2	49.0	51.0
9.5	37.5	37.5	25.0	0.0	75.0	2 5.0	62.5	37.5	37.5	62.5
12.5	50.0	0.0	50.0	0.0	50.0	50.0	100.0	0.0	50.0	50.0
1.18	17.9	21.4	32.1	28.6	39.3	60.7	50.0	50.0	50.0	50.0
2.36	17.3	19.1	23.6	**40.0**	36.4	63.6	40.9	59.1	51.8	48.2
4.75	26.8	26.8	26.8	19.5	53.7	46.3	53.7	46.3	50.0	50.0
9.5	**44.4**	22.2	22.2	11.1	66.7	33.3	66.7	33.3	44.4	55.6
12.5	0.0	0.0	100.0	0.0	0.0	100.0	100.0	0.0	100.0	0.0
1.18	27.5	23.2	27.5	21.7	50.7	49.3	55.1	44.9	50.7	49.3
2.36	17.0	24.0	32.0	27.0	41.0	59.0	49.0	51.0	48.0	52.0
4.75	20.9	29.1	25.5	24.5	50.0	50.0	46.4	53.6	50.0	50.0
9.5	30.0	40.0	10.0	20.0	70.0	30.0	40.0	60.0	40.0	60.0
1.18	27.0	22.5	23.6	27.0	49.4	50.6	50.6	49.4	62.9	37.1
2.36	21.8	17.9	23.1	**37.2**	39.7	60.3	44.9	55.1	47.4	52.6
4.75	26.6	28.7	19.1	25.5	55.3	44.7	45.7	54.3	51.1	48.9
9.5	9.1	**45.5**	36.4	9.1	54.5	45.5	45.5	54.5	54.5	45.5
1.18	21.1	21.1	22.5	**35.2**	42.3	57.7	43.7	56.3	60.6	39.4
2.36	26.8	21.1	24.4	27.6	48.0	52.0	51.2	48.8	49.6	50.4
4.75	12.6	31.6	26.3	29.5	44.2	55.8	38.9	61.1	43.2	56.8
9.5	**41.7**	25.0	16.7	16.7	66.7	33.3	58.3	41.7	50.0	50.0

6. CONCLUSION

Use of experimental and image processing techniques on evaluating durability and permeability of selected OGFC mixtures to analyse relationships towards obtaining more durable and permeable OGFC and enhancing OGFC as a pavement material was the major aim of this study. Based on the research findings, the followings can be summarized as conclusions.

1. The selected gradations in this study were addressed as A, B and C. When it comes to the experimental program, the gradation type A showed a lower abrasion loss and type C showed the highest loss. This means gradation type A specimens are comparatively more durable. The permeability test indicated that the OGFC type C is more permeable and A has the lowest permeability. However, the permeability difference between A and B specimens were minor. Therefore, type B can be selected as the optimum considering both durability and permeability criteria.
2. A segregation of an OGFC specimen was analysed in vertical direction. This was carried out developing statistics of aggregate numbers and areas of all six cross sections of a specimen which allowed to quantify the level of segregation.
3. Segregation in the horizontal direction was observed using different aggregate proportions on cross sections. This was done using Delaunay distance calculation process, which enabled the calculation of distance between selected size aggregates.
4. Quantification of horizontal segregation carried out by developing statistic of number of aggregates belongs to different areas in the cross section. However, it can be recommended that, further extension and enhancement of the algorithm used to calculate Delaunay triangles, can be developed to identify horizontal segregation more precisely.
5. The developed program can also be used to check the quality of an OGFC field specimen when the program is fed with all the design stage data. This can be used to check the level of differences between aggregate arrangements of designs and field specimens.
6. The relationship between permeability and total number interconnected voids was a directly proportional, linear behaviour. However, total voids could not provide a linear behaviour with permeability.

7. Two interconnected void prediction models were developed and path index of both models provided a linear relationship with permeability while Model 02 showed a more proportionate behaviour.
8. Mathematically processed data from raw images were imported on software programs for 3D visualization. These developed 3D models supported to visually observe the internal void network, aggregate packing, number of voids variation through the depth of the OGFC specimens more meaningfully.

7. REFERENCES

3D Line Plots | Python | Plotly. (2021). https://plotly.com/python/3d-line-plots/

3D Scatter Plots | Python | Plotly. (2021). https://plotly.com/python/3d-scatter-plots/

Alvarez-Lugo, A. E., Reyes-Ortiz, O. J., & Miró, R. (2014). A review of the characterization and evaluation of permeable friction course mixtures Revisión de la caracterización y evaluación de mezclas drenantes. *Ingeniare. Revista Chilena de Ingeniería*, *22*(4), 469–482.

Alvarez, A. E., Amy, ;, Martin, E., Asce, M., & Estakhri, C. (2010). Drainability of Permeable Friction Course Mixtures. *Journal of Materials in Civil Engineering*, 556–564. https://doi.org/10.1061/ASCEMT.1943-5533.0000053

Anderson, K. W., Uhlmeyer, J. S., Sexton, T., Rusell, M., & Weston, J. (2013). Summary Report on the Performance of Open Graded Friction Course Quieter pavements. In *WSDOT Research Report WA-RD 817.1* (Issue September 2013).

Bessa, I. S., Castelo Branco, V. T. F., & Soares, J. B. (2012). Evaluation of different digital image processing software for aggregates and hot mix asphalt characterizations. *Construction and Building Materials*, *37*, 370–378. https://doi.org/10.1016/j.conbuildmat.2012.07.051

Chen, J., Li, H., Huang, X., & Wu, J. (2015). Permeability Loss of Open-Graded Friction Course Mixtures due to Deformation-Related and Particle-Related Clogging: Understanding from a Laboratory Investigation. *Journal of Materials in Civil Engineering*, *27*(11), 04015023. https://doi.org/10.1061/(asce)mt.1943-5533.0001282

Chen, X., Zhu, H., Dong, Q., & Huang, B. (2017). Case study: performance effectiveness and cost-benefit analyses of open-graded friction course pavements in Tennessee. *International Journal of Pavement Engineering*, *18*(11), 957–970. https://doi.org/10.1080/10298436.2016.1138112

Chen, Y., Tebaldi, G., Roque, R., Lopp, G., & Su, Y. (2012). Effects of interface condition characteristics on Open-Graded Friction Course top-down cracking performance. *Road Materials and Pavement Design*, *13*(SUPPL. 1), 56–75. https://doi.org/10.1080/14680629.2012.657051

Coleman O'Flaherty, D. H. (2015). *Highways: The Location, Design, Construction and Maintenance of Road Pavements* (5th ed.). ICE Publishing.

Coleri, E., Kayhanian, M., Harvey, J. T., Yang, K., & Boone, J. M. (2013). Clogging

evaluation of open graded friction course pavements tested under rainfall and heavy vehicle simulators. *Journal of Environmental Management*, *129*, 164–172. https://doi.org/10.1016/j.jenvman.2013.07.005

Fang, M., Park, D., Singuranayo, J. L., Chen, H., & Li, Y. (2019). Aggregate gradation theory, design and its impact on asphalt pavement performance: a review. *International Journal of Pavement Engineering*, *20*(12), 1408–1424. https://doi.org/10.1080/10298436.2018.1430365

Hassan, H. F., & Al-Jabri, K. S. (2005). Effect of organic fibers on open-graded friction course mixture properties. *International Journal of Pavement Engineering*, *6*(1), 67–75. https://doi.org/10.1080/10298430500087936

Joni, H. H., Alwan, I. A., & Naji, G. A. (2020). Investigations of the road pavement surface conditions using MATLAB image processing. *IOP Conference Series: Materials Science and Engineering*, *737*(1), 0–9. https://doi.org/10.1088/1757-899X/737/1/012133

Kabir, M. S., King, W., Abadie, C., Icenogle, P., & Cooper, S. B. (2012). Louisiana's experience with Open-graded friction course mixtures. *Transportation Research Record*, *2295*, 63–71. https://doi.org/10.3141/2295-08

Kim, K., & Kang, M. (2018). Linking the effect of aggregate interaction to the compaction theory for asphalt mixtures using image processing. *Applied Sciences (Switzerland)*, *8*(11). https://doi.org/10.3390/app8112045

King, W., Kabir, S., Cooper, S. B., & Abadie, C. (2013). Evaluation of Open Graded Friction Course (OGFC). *Louisiana Transportation Research Center (LTRC) Report FHWA/LA.13/513*, *2*, 72.

Kowalski, K. J., McDaniel, R. S., Shah, A., & Olek, J. (2009). Long-term monitoring of noise and frictional properties of three pavements: Dense-graded asphalt, stone matrix asphalt, and porous friction course. *Transportation Research Record*, *2127*, 12–19. https://doi.org/10.3141/2127-02

Kumar Rathore, A. (2017). Comprehensive Review of Data Visualization Techniques using Python. *Amity Journal of Computational Sciences (AJCS)*, *3*(2), 42–48. www.amity.edu/ajcs

Liu, Y., Su, P., Li, M., You, Z., & Zhao, M. (2020). Review on evolution and evaluation of asphalt pavement structures and materials. *Journal of Traffic and Transportation Engineering (English Edition)*, *7*(5), 573–599. https://doi.org/10.1016/j.jtte.2020.05.003

Mampearachchi, W. K., Masakorala, S. R., & Umasangar, K. (2019). Aggregate interlocking of open-graded friction courses with compaction effort. *Journal of the National Science Foundation of Sri Lanka*, *47*(1), 139–146. https://doi.org/10.4038/jnsfsr.v47i1.8931

Mejias de Pernia, Y., & Gunaratne, M. (2017). Application of perceptual image coding and the neural network method in predicting the optimum Asphalt binder content of open-graded friction course mixtures. *Road Materials and Pavement Design*, *18*(1), 38–63. https://doi.org/10.1080/14680629.2016.1139499

Onyango, M., Asce, M., & Woods, M. (2017). Analysis of the Utilization of Open-Graded Friction Course (OGFC) in the United States. *Airfield and Highway Pavements*, 137–147.

Pathak, S., Choudhary, R., Kumar, A., & Kumar Shukla, S. (2020). Evaluation of Benefits of Open-Graded Friction Courses with Basic Oxygen Furnace Steel-Slag Aggregates for Hilly and High-Rainfall Regions in India. *Journal of Materials in Civil Engineering*, *32*(12), 04020356. https://doi.org/10.1061/(asce)mt.1943-5533.0003445

Pereira, P., & Pais, J. (2017). Main flexible pavement and mix design methods in Europe and challenges for the development of an European method. *Journal of Traffic and Transportation Engineering (English Edition)*, *4*(4), 316–346. https://doi.org/10.1016/j.jtte.2017.06.001

Reyes-Ortiz, O. J., Mejia, M., & Useche-Castelblanco, J. S. (2021). Digital image analysis applied in asphalt mixtures for sieve size curve reconstruction and aggregate distribution homogeneity. *International Journal of Pavement Research and Technology*, *14*(3), 288–298. https://doi.org/10.1007/s42947-020-0315-6

Takahashi, S. (2013). Comprehensive study on the porous asphalt effects on expressways in Japan: based on field data analysis in the last decade. *Http://Dx.Doi.Org/10.1080/14680629.2013.779298*, *14*(2), 239–255. https://doi.org/10.1080/14680629.2013.779298

Wang, Lan, Xing, Y., & Chunqing, C. (2009). The Noise-reducing Character of OGFC pavement with Crumb rubber modified Asphalt. *International Conference on Transportation Engineering*.

Wang, Liang, Rizvi, H. R., Khattak, M. J., & Gang, D. D. (2011). Development and Evaluation of Functional Open Graded Friction Courses (FOGFC) Mixtures for In Situ Highway Runoff Treatment. *Geo-Frontiers* .

Zelelew, H. M., Zelelew, H. M., Papagiannakis, A. T., & Masad, E. (2008). Application of Digital Image Processing Techniques for Asphalt Concrete Mixture Images Simulation of Plastic Deformation Behavior View project Energy Harvesting from Pavement Infrastructure View project Application of Digital Image Processing Techniques for Asphalt Concrete Mixture Images. *International Association for Computer Methods and Advances in Geomechanics* . https://www.researchgate.net/publication/242222597

Zhu, S., Liu, X., Cao, Q., & Huang, X. (2017). Numerical Study of Tire Hydroplaning Based on Power Spectrum of Asphalt Pavement and Kinetic Friction Coefficient. *Advances in Materials Science and Engineering*, *2017*. https://doi.org/10.1155/2017/5843061